Neurobiology of Disease 130 (2019) 104486

Contents lists available at ScienceDirect

Neurobiology of Disease

journal homepage: www.elsevier.com/locate/ynbdi

The critical role of ASD-related gene *CNTNAP3* in regulating synaptic development and social behavior in mice

Da-li Tong[a,c,1], Rui-guo Chen[b,c,1], Yu-lan Lu[d], Wei-ke Li[a,c], Yue-fang Zhang[a], Jun-kai Lin[a], Ling-jie He[a], Ting Dang[d], Shi-fang Shan[a], Xiao-Hong Xu[a], Yi Zhang[f], Chen Zhang[f], Ya-Song Du[e], Wen-Hao Zhou[d], Xiaoqun Wang[b,c,*], Zilong Qiu[a,c,*]

[a] *Institute of Neuroscience, State Key Laboratory of Neuroscience, CAS Center for Excellence in Brain Science and Intelligence Technology, Chinese Academy of Sciences, Shanghai, China*
[b] *Institute of Biophysics, State Key Laboratory of Brain and Cognitive Sciences, CAS Center for Excellence in Brain Science and Intelligence Technology; Chinese Academy of Sciences, Beijing, China*
[c] *The College of Life Science, University of Chinese Academy of Sciences, Beijing, China*
[d] *Department of Neonatology, Children's Hospital of Fudan University, Shanghai, China*
[e] *Shanghai Mental Health Center, Shanghai Jiao Tong University School of Medicine, Shanghai, China*
[f] *State Key Laboratory of Membrane Biology, PKU-IDG/McGovern Institute for Brain Research, School of Life Sciences; Peking University, Beijing, China*

ARTICLE INFO

Keywords:
Autism spectrum disorders
CNTNAP3
Autism spectrum disorders
Spatial learning
Repetitive behaviors

ABSTRACT

Accumulated genetic evidences indicate that the contactin associated protein-like (CNTNAP) family is implicated in autism spectrum disorders (ASD). In this study, we identified genetic mutations in the *CNTNAP3* gene from Chinese Han ASD cohorts and Simons Simplex Collections. We found that CNTNAP3 interacted with synaptic adhesion proteins Neuroligin1 and Neuroligin2, as well as scaffolding proteins PSD95 and Gephyrin. Significantly, we found that CNTNAP3 played an opposite role in controlling the development of excitatory and inhibitory synapses *in vitro* and *in vivo*, in which ASD mutants exhibited *loss-of-function* effects. In this study, we showed that the male *Cntnap3*-null mice exhibited deficits in social interaction , spatial learning and prominent repetitive behaviors. These evidences elucidate the pivotal role of CNTNAP3 in synapse development and social behaviors, providing mechanistic insights into ASD.

1. Introduction

Autism spectrum disorder (ASD) is a prevalent neurodevelopmental disorder with early onset in the childhood, characterized by deficits in social behaviors and prominent repetitive behaviors. Numerous genes have been discovered to associate with ASD by human genetic studies. Notably, it has been reported that mutations in genes encoding synaptic adhesion molecules, including neuroligin (NLGN) and neurexin (NRXN) family members, are closed related to ASD (Feng et al., 2006; Jamain et al., 2003; Kim et al., 2008), which are often found in ASD patients, suggesting that the synaptic dysfunction significantly contribute to ASD (de la Torre-Ubieta et al., 2016; Huguet et al., 2013; Szatmari et al., 2007; Willsey and State, 2015).

As a member of NRXN superfamily, the contactin associated protein-like (CNTNAP) family (also known as the CASPR protein family) has been identified to be associated with ASD, especially CNTNAP2 and CNTNAP4. The CNTNAP family contains 5 members from CNTNAP1 to CNTNAP5, featured by multiple repeats of epidermal growth factor (EGF) domains and laminin G (LamG) domains in the extracellular domains, as well as the intracellular PDZ (Postsynaptic density 95, Discs large, Zonula occludens-1)-binding domain (Bellen et al., 1998; Peles et al., 1997; Spiegel et al., 2002; Traut et al., 2006). CNTNAP1 and CNTNAP2 are involved in the formation of myelin and trafficking potassium channels of the cell membrane (Poliak et al., 2003; Rios et al., 2000; Traka et al., 2003). CNTNAP2 are also involved in the neurite and synapse development. When knocking down the *Cntnap2* in cultured neurons, the total neurite length was decreased (Anderson et al., 2012). Furthermore, the spine density was decreased in the *Cntnap2*$^{-/-}$ mice (Varea et al., 2015). CNTNAP3 was highly expressed in cortex and hippocampus of the mouse postnatal brain at P7 and P14 (Hirata et al., 2016a), and *Cntnap3* knockout mice exhibited the normal motor function and anxiety level with a little disability of motor learning in the

* Corresponding authors at: The College of Life Science, University of Chinese Academy of Sciences, Beijing, China.
E-mail addresses: xiaoqunwang@ibp.ac.cn (X. Wang), zqiu@ion.ac.cn (Z. Qiu).
[1] These authors contribute equally to this work.

https://doi.org/10.1016/j.nbd.2019.104486
Received 7 January 2019; Received in revised form 3 May 2019; Accepted 27 May 2019
Available online 29 May 2019
0969-9961/

rota-rod test (Hirata et al., 2016b). CNTNAP4 is fateful for the formation of axo-axonic synapse by interacting with Contactin5 in the peripheral nervous system (Ashrafi et al., 2014). Whereas in the central nervous system, CNTNAP4 plays a vital part in regulating synaptic transmission of GABAergic neurons. Little was known about the function of CNTNAP5.

Genetic studies suggested that the CNTNAP2 gene had strong connections with ASD (Alarcon et al., 2008; Arking et al., 2008; Bakkaloglu et al., 2008). The CNTNAP2 protein plays a critical role in neural development and synaptic transmission. Furthermore, *Cntnap2* null mice exhibited various autistic-like behaviors (Anderson et al., 2012; Penagarikano et al., 2011). Moreover, the *de novo* (Q693R, N1082Y, D1148N) and inherited (H513R) mutations of CNTNAP4 were found in the ASD patients (Li et al., 2017; Lim et al., 2017; Iossifov et al., 2014). The *Cntnap4* knockout mice showed heavily stereotypic behaviors like self-grooming (Karayannis et al., 2014). The *de novo* (P714R, T919 M, V1168I, T1195 M) and inherited (R1234Q) mutations of CNTNAP5 were found in the ASD patients previously (Pagnamenta et al., 2010; Vaags et al., 2012).

The whole-genome sequencing of 476 autism families from the Simons Simplex Collection detected a stop-gain *de novo* mutation in CNTNAP3 (R1219X) in an ASD proband (Turner et al., 2017). An inherited mutation, G410S of CNTNAP3 was also found in the ASD patient (Vaags et al., 2012). Notably, CNTNAP3 was found to express differentially in the blood of individuals with autism (Kong et al., 2012). Furthermore, a deletion of 9p12 which contains *CNTNAP3* was found in one mental retardation (MR) patient (Mosrati et al., 2012). Taken together, CNTNAP3 may be a candidate gene for autism spectrum disorders.

In this study, we identified genetic mutations in the *CNTNAP3* gene through whole-exome sequencing in Chinese Han ASD cohorts and Simons Simplex Collections. To address molecular mechanisms underlying CNTNAP3 regulating synaptic development and social behaviors, we performed extensive molecular, physiological and genetic experiments. We found that CNTNAP3 interacted with critical synaptic adhesion molecules such as Neuroligin1 and Neurogligin2 proteins, as well as postsynaptic scaffolding protein PSD95 and Gephyrin. More importantly, our data demonstrated that CNTNAP3 played an opposite role in controlling development of excitatory and inhibitory synapses *in vitro* and *in vivo*. Knocking down of *Cntnap3* led to decrease of excitatory synapse formation and increase of the inhibitory synapse formation, while ASD mutants exhibited *loss-of-function* effects. Furthermore, *Cntnap3*$^{-/-}$ mice exhibited deficits in social behavior, cognitive tasks and prominent repetitive behaviors, confirming the role of CNTNAP3 in ASD.

2. Materials and methods

2.1. Ethics statement

We obtained assent from the Institutional Review Board (IRB), Shanghai Mental Health Center of Shanghai Jiao Tong University (FWA Number: 00003065; IROG Number: 0002202). Dr. Yi-Feng Xu approved and signed our study with ethical review number 2016–4. Written informed consent was obtained from parents in consideration of the fact that all patients were minors. All participants were screened using the appropriate protocol approved by the IRB. Subjects' information and Clinical Scale Assessment was described in previous report (22). The criteria of genetic testing are approved by the ethics committees of Children's Hospital, Fudan University (2014–107). Pre-test counseling were performed by physicians, appropriate informed consents were signed by patient's parents in clinics.

2.2. Simons simplex collection data

We are grateful to all of the families at the participating Simons Simplex Collection (SSC) sites, as well as the principal investigators (A. Beaudet, R. Bernier, J. Constantino, E. Cook, E. Fombonne, D. Geschwind, R. Goin-Kochel, E. Hanson, D. Grice, A. Klin, D. Ledbetter, C. Lord, C. Martin, D. Martin, R. Maxim, J. Miles, O. Ousley, K. Pelphrey, B. Peterson, J. Piggot, C. Saulnier, M. State, W. Stone, J. Sutcliffe, C. Walsh, Z. Warren, E. Wijsman).

Approved researchers can obtain the SSC population dataset described in this study (https://simons.wuxinextcode.com/csa/welcome) by applying at https://base.sfari.org.

2.3. Animals

All of the mice used in the experiment were in the background of C57BL/6 J (RRID: IMSR_JAX:000664). The mice were fed, bred and been experimented in SPF (Specific Pathogen Free) facilities on a 12:12 light-dark (light: 0:00 to 12:00, dark: 12:00 to 24:00) cycle at room temperature (22 °C). Except the embryonic mice used in the cell culture, all of the mice were male. *Cntnap3* knockout and *Cntnap3* conditional knockout mice were customized designed and ordered from Biocytogen in the C57BL/6 J background. The NEX-Cre mice (Kashani et al., 2006) expressed Cre in the excitatory neurons of cerebral cortex and hippocampus. vGat-IRES-Cre mice were bought from the Jackson laboratory (Stock No: 016962, RRID: IMSR_JAX:016962) which expressed Cre to inhibitory GABAergic neuron. The mice were crossed with C56BL/6 J mice for > 10 generations before using. The mice used in the behavioral tests were from 2 month to 4 month. The mice used in the PV and SST staining were P14. The mice used in the Golgi staining were from 2 to 4 months old. The mice used in the electrophysiology were from 2 to 4 months old (adult) or from P14 to P21 (the adolescent group).

2.4. Plasmid construct

The plasmids of pCAG-NL1(−) and pNICE-NL2(−) were bought from Addgene (Addgene number: pCAG-NL1(−): 15260, pNICE-NL2(−) 15,246). The plasmids of pCAG-GFP-PSD95, pCAG-GFP-Gephyrin and pCAG-HA-Shank3 were gift from Dr. Xiang Yu (Institute of Neuroscience, CAS, Shanghai, China). The sequence of human-CNTNAP3 (NM_033655.3) was generated in the PRK5 and pCAGGS vector. The LamG vector contained the last LamG domain, transmembrane region and PDZ-binding domain of human-CNTNAP3 (from amino acid Phe1046 to Cys1288). The shRNA was generated in FUGW-H1 vector (Addgene number: 25870).

The mouse CNTNAP3 RNAi sequence: CAGACAGTGTGGTACAATA.

The DsRed RNAi sequence was used as control:AGTTCCAGTACGG CTCCAA.

2.5. Tissue separation

The C57BL/6 J mice were deeply anaesthetized with 0.14 g/kg sodium pentobarbital. Brains were quickly moved into the PBS (Phosphate Buffer Saline, CORNING, 21–040-CVR) solution in 4 °C. The different regions of brain were separated in the PBS solution under the guide of The Mouse Brain in Stereotaxic Coordinates (Academic Press, 2001).

2.6. RNA isolation and reverse transcription

The 0.1 g tissue was put in 1 mL Trizol (Invitrogen, 15,596,018) and then crushed thoroughly in the ice-water bath. Total RNA was isolated using the method of user guide of TRIzol™ Reagent. Reverse-transcribed using the Reverse Transcriptase M-MLV kit (TaKaRa, D2639B). 1 μg total mRNA and 50 nmol oligo dT (12–18 primers) were used in the reverse transcription.

2.7. Quantitative real-time RT-PCR (qPCR)

Quantitative real-time RT-PCR was used for investigating the mRNA level of *Cntnap3*.

For qPCR analysis, the gene expression of cDNA sample was analyzed using SYBR green (Toyobo, QPK-201). The following primers were used:

mouse-CNTNAP3: forward: TCAAAACCGGGCTAGAGTCA.

reverse: GGGGCTGTCTATCTTCTGCG.

mouse-GAPDH: forward: ACGGCCGCATCTTCTTGTGCAGTG.

reverse: GGCCTTGACTGTGCCGTTGA.

The qPCR program was three steps with melt as follows: 95 °C denaturation for 10 min, followed by 40 cycles of 95 °C for 10 s, 60 °C for 15 s, and 72 °C for 20 s. CNTNAP3 level was calculated and standardized by using the ΔCt method and GAPDH expression level as control.

2.8. In situ hybridization

In situ hybridization was used for investigating the expression pattern of *Cntnap3* mRNA in different region of the mice brain.

mRNA probe preparation: the mRNA probe was the same probe used in the Allen Brain (experiment number: 70566223). The mRNA probe was constructed in the T vector and transcript with T7 RNA polymerase (Promega, P2077). 4 μg DNA was used to do the transcript and Incubate for 4 h at 37 °C.

Perfuse mouse with 20 mL cold DEPC-PBS and then 20 mL cold 4% DEPC-PFA, then move in 20 mL cold 4% DEPC-PFA. Postfix brain in 4% DEPC-PFA at 4 °C overnight. Move the brain to the 15% Sucrose-DEPC-PBS for 24 h. Then move the brain to 30% Sucrose-DEPC-PBS for 48 h. Embed the brain in OCT (Optimal Cutting Temperature, *SAKURA*, 4583) and freeze it in −22 °C for 1 h. Coronal section brain at 40 μm with Leica CM-1950 and collect slices into cold DEPC-PBS.

Wash 10 mins at RT with DEPC-PBS. Then wash twice 5 min at RT (Room Temperature) with DEPC-PTw (PBS-Tween PBS with 0.1% Tween). Wash 30 mins at RT with 0.5% Triton in 2× SSC and twice 5 mins with DEPC-PTw. After acetylating for 10 mins on the rocker with fresh Acetylation mix (0.1 M Triethanolamine, 0.25% Acetic anhydride), wash three times 5 mins with DEPC-PBS. Pre-hybridize in rinse-prehybridization (50% Formamide, 5× SSC, 0.1% Tween-20, 0.1% CHAPS, 5 mM EDTA) for 2 h in 65 °C and then hybridize at 65 °C overnight in 1 μg/ml probe with hybridization (50% Formamide, 5× SSC, 0.3 mg/ml yeast tRNA, 100 mg/ml heparin, 1× Denhardt's, 0.1% Tween-20, 0.1% CHAPS, 5 mM EDTA).

The next day, rinse with 65 °C rinse- prehybridization and wash 30 mins at 65 °C with rinse- prehybridization. Wash 30 mins at 65 °C with 1:1 rinse-prehybridization/TBST. After washing twice 5 mins with TBST. Rinse with 1:1 TBST/TAE, wash three times 5 mins with TAE. Transfer slices to wells in 2% agarose/TAE gel. Run gel at 60 V for 2 eh. Rinse twice with TBST. Incubate overnight at 4 °C in 1:1000 anti-dig antibody (Roche, 11,093,274,910, RRID:AB_514497) in blocking reagent (0.5% BSA (Albumin from Bovine Serum) in B1 buffer (0.1 M Tris, pH 7.5, 0.15 M NaCl)).

The next day, wash 15 mins with TBST 6 times. Stain the sections in fast red solution (HNPP fluorescent detection set, Roche, 11,758,888,001) for > 3 h in blocking reagent. For the *Cntnap3 in situ* hybridization with PV Immunohistochemical staining, incubate overnight at 4 °C in 1:1000 anti-PV antibody (Millipore, MAB157, RRID: AB_2174013) in blocking reagent. Wash 15 mins with TBST 3 times. Stain the sections with 1:1000 Donkey anti mouse CF488A conjugate (Biotium, 20,014, RRID:AB_10561327).

2.9. 293 T cell culture and co-immunoprecipitation

Co-immunoprecipitation was used for investigating the protein interaction of CNTNAP3 and other synapse protein.

293 T cell was cultured in the DMEM (Gibco, 11,965–092) medium with 10% FBS on 6-well plates for biochemical experiments. The cells were transfected by Lipo-2000 (Invitrogen, 11,680–019) with 2 μg of each vector 24 h after planting. After 2 days of transfection, the cells were lysed in RIPA buffer (1%Triton, 150 mM NaCl, 25 mM Tris-Hcl (pH = 7.4), 2 mM EDTA (pH = 8.0)) for 1.5 h at 4 °C. After the Sonic broken of 10 min and 5000 rpm centrifuge for 10 min, the supernatant was collected and added with protein A/G agarose (Abmart, A10001M) with IgG or anti-GFP (Green Fluorescent Protein, Abmart, A20004L), anti-HA-tag mouse mAb agarose conjugated (Abmart, M20013S) or anti-myc-tag mouse mAb agarose conjugated (Abmart, M20012S) and rotated for 4 h. Wash the agarose conjugated beads 3 times (rotated 10 mins, 5000 rpm centrifuge 2 mins) with RIPA buffer before loading the protein by loading buffer.

2.10. Western blot

8% SDS-polyacrylamide gel (8% acrylamide mix, 0.375 M Tris (pH 8.8), 0.1% SDS, 0.1% APS, 0.06%TEMED) was used in the western blot. SDS-polyacrylamide gel electrophoresis method was 80 V 30mins and then 120 V 90 mins. Proteins were transferred onto the Immobilon polyvinylidene difluoride membrane (Millipore) for 90mins at 200 mA. The membrane was blocked by TBST solution (50 mM Tris-HCl, pH 7.5, 150 mM NaCl, and 0.1% Tween 20) with 3% BSA and 3% skim milk powder for 4 h at RT and incubated overnight at 4 °C with primary antibody solution.

The next day, Wash 3 times 15 mins with TBST. The membrane was treated with secondary antibody for 2 h at RT. Wash 15 mins with TBST 3 times. The reaction was analyzed by using imaging film. Antibodies used were as following: Anti-HA: 1:1000 (Covance, MMS-101R, RRID:AB_291262), Anti-Myc: 1:1000 (Abmart, M2002 L), Anti-GFP: 1:1000 (Abmart, A20004L), Sheep anti mouse HRP: 1:5000 (GE-Healthcare, NA931V).

2.11. Primary cultures of cortical neurons

Primary cultures of cortical neurons, calcium phosphate transfection and immunohistochemical staining were used for investigating the synapse changes *in vitro*.

Mouse cortical neurons were cultured from 13.5 day embryos of either sex (Yu and Malenka, 2003). Cerebral cortices were dissected, dissociated, and cultured in 0.5 mL/well Neurobasal medium (Gibco, 21103-049) with 0.2% B27 (Gibco, 17504-044) and 2 mM Glutamax-I (Gibco, 35050-061)on Lab-Tek II Chamber Slide (Thermo Fisher Scientific, 154,941) at 100,000 cells/cm^2. After transfection, feed the cultures 50% with new medium every 2 days. For the axon experiment, the cells were transfected by Lipo-2000 with 1 μg of each vector 18 h after planting. For the dendrite and spine experiment, the cells were transfected by calcium phosphate transfection with 2 μg of each vector 5 days after planting.

2.12. Calcium phosphate transfection

The transfection was done at day 5 after planting. The Day before transfection feed the cultures 50% with new medium and save the conditioned medium from the cultures in the fridge. In a 1.5 ml Eppendorf tube, mix DNA and $CaCl_2$. For each well: 1.9 μL 2 M $CaCl_2$, 2 μg DNA for each vector in water, add water to 15 μL. Add 15 μL pH 7.05 2× HBS (274 mM NaCl, 10 mM KCl, 1.4 mM Na_2HPO_4, 15 mM glucose, 42 mM HEPES) per transfection slowly, while flickering the tube containing DNA. Hold the tubes shielded away from light for 30 min at room temperature. Remove 0.25 mL of media from each well and pool with conditioned medium from the day before. Add 30ul of the transfection mixture to each plate, dripping slowly to cover the cells. After 90 mins, wash neurons twice with wash buffer (pH 7.4, 1 mM $CaCl_2$, 0.8 mM MgSO4, 5.3 mM KCl, 120 mM NaCl, 10 mM HEPES and 25 mM Glucose). Add back the 0.5 mL conditioned media to each well.

2.13. Immunohistochemical staining

Cultured neurons: After wash with PBS for 5 mins, the neurons were fixed in 4% PFA at room temperature for 20 min. Wash twice 10 mins with PBS. Block the cell with antibody buffer (3% BSA and 0.1% Triton-X100 in PBS) for 1 h. In the vGlut1 and vGat experiment, Triton-X100 was not added in the antibody buffer. Incubate overnight at 4 °C with primary antibody in blocking buffer. Wash 3 times 15 mins with PBS; incubate at RT with secondary antibody and 1:1000 DAPI in antibody buffer for 2 h. Wash 3 times 15 mins with PBS.

Slice: The mice were deeply anaesthetized with 0.14 g/kg sodium pentobarbital. 20 mL PBS and then 20 mL 4% PFA were used to perfuse; then move in 20 mL 4% PFA for overnight. Move the brain to 15% sucrose in PBS for 24 h and to 30% sucrose in PBS for > 2 days. Embed the brain in OCT and freeze it in −22 °C for 1 h. Section brain at 40 μm with Leica CM-1950 and collect slices into cold PBS. Wash twice 10 mins with PBS. Block the cell with block buffer (5% BSA and 0.3% Triton-X100 in PBS) for 1 h. Incubate overnight at 4 °C with primary antibody in antibody buffer. Wash 3 times 15 mins with PBS; incubate at RT with secondary antibody and 1:1000 DAPI in antibody buffer for 2 h. Wash 15 mins with PBS 3 times.

Antibodies used were as following: GFP (Rabbit): 1:1000 (Invitrogen, A11122, RRID:AB_221569), GFP (Mouse): 1:1000 (Earthox, E022030–10), vGlut1 (Vesicular Glutamate Transporter1): 1:3000 (Millipore, AB5905, RRID:AB_2301751), vGat (Vesicular GABA Transporter): 1:1000 (Synaptic Systerms, 131,002, RRID:AB_887871), PV (Parvalbumin): 1:1000 (Millipore, MAB157, RRID:AB_2174013), SST (Somatostatin): 1:250 (Santa Cruz, SC-7819, RRID:AB_2302603), Donkey anti mouse CF488 conjugate (Biotium, 20,014, RRID:AB_10561327), Donkey anti rabbit CF488 conjugate (Biotium, 20,015, AB_10559669), Donkey anti mouse CF555 conjugate (Biotium, 20,037, RRID: AB_10559035), Goat anti guinea pig CF555 (conjugate, Biotium, 20,036, RRID:AB_10557404), Donkey anti rabbit CF647 conjugate, (Biotium, 20,047, RRID:AB_10853792).

In the axon and dendrite experiment, the total axon length, total dendrite length and branch number were analyzed by Image J (RRID:SCR_003070). The total axon length and total dendrite length were counted from the soma to the terminal. The branch number equaled to the number of the dendrite terminal. In the synapse density experiment, the head of spine or the diameter of vGlut, vGat puncta was > 0.5 μm was collected and analyzed with the collected dendrite > 20 μm.

2.14. Golgi staining

Golgi staining was used for investigating the synapse density *in vivo*.

The age-matched mice were deeply anaesthetized with 0.14 g/kg sodium pentobarbital. Perfuse mouse with 20 mL PBS and the brains were quickly removed and Golgi staining buffer (1:1 solution A/solution B) was performed 1 day before by using the FD Rapid GolgiStainTM Kit (FD NeuroTechnologies, PK401). Change the Golgi staining buffer 1 day after perfusion and then then staining for another 13 days (total staining for 14 days). Move the brains to solution C for 5 days. Section brain at 100 μm and collect slices into the gelatin coated glass slide. The staining steps were according to the manufacturer's instructions. At least 3 mice from 2 different litters and at least 6 slices for each mouse were used in the experiment. The dendrite collected in the synapse experiment must be > 20 μm.

2.15. Electrophysiological recordings in slices

Mice were anaesthetized with avertin and decapitated. The brain was quickly removed and submerged in oxygenated (95% O_2 and 5% CO_2) ice-cold sucrose-based artificial cerebrospinal fluid (sucrose-based aCSF() containing (in mM: 234 Sucrose, 2.5 KCl, 26 $NaHCO_3$, 1.25 NaH_2PO_4, 11 D-Glucose, 0.5 $CaCl_2$ and 10 $MgSO_4$). Coronal slices (300 um) were prepared using a vibratome (VT1200S, Leica) and kept in an incubating chamber filled with oxygenated aCSF (in mM: 126 NaCl, 3 KCl, 26 $NaHCO_3$, 1.2 NaH_2PO_4, 10 D-Glucose, 2.4 $CaCl_2$ and 1.3 $MgCl_2$) at 34 °C. After a recovery period at least 40 min, an individual slice was transferred to a recording chamber and was continuously super fused with oxygenated aCSF at a rate of 3–5 mL per minute at 30 ± 1 °C. An inverted microscope (Andor) equipped with epifluorescence and infrared-differential interference contrast (DIC) illumination, a camera, and one air immersion lense (4×) and one water immersion lense (40×) were used to visualize and target recording electrodes and cells.

Whole-cell patch clamp recording was performed on cells from the layer 5 of neocortex and CA1 of hippocampus. Patch pipettes had a 5–7 MΩ resistance when filled with intracellular solution (in mM: 130 potassium gluconate, 16 KCl, 2 $MgCl_2$, 10 HEPES, 0.2 EGTA, 4 Na_2-ATP, 0.4 Na_3-GTP, pH = 7.25, adjusted with KOH). Inward currents were recorded in voltage-clamp mode with a basal holding potential of −60 mV followed by stimulating pulses from −80 mV to 60 mV with a step size of 10 mV. Evoked action potentials were recorded in current-clamp mode using a series of depolarizing currents ranged from −100 pA to 280 pA in increments of 20 pA.

1 μm TTX was added to the extracellular solution and extracellular Mg2+ was reduced to 5 μM (Lee et al., 2007) when measuring both mEPSCs and mIPSCs. While measuring mIPSCs, we hold membrane potential at 12 mV to eliminate mEPSC. While measuring mEPSCs, we hold membrane potential at -70 mV to eliminate mIPSCs. And mEPSCs were also isolated by local application of 20 μM of bicuculline methiodide (BMI).

Stimulus delivery and data acquisition were conducted with a multiclamp 700B amplifier and a Digidata 1440A (Molecular Devices), which were controlled by Clampex 10.2 (Molecular Devices).

2.16. Behavioral tests

All the mice used in the behavioral tests were male and handled for > 3 days prior to behavioral tasks. The animals' behaviors were recorded and analyzed by Ethovision XT software (Noldus, Wageningen, Netherlands, RRID:SCR_000441) or the experimenter that do not know the genotype of the mice. Before any behaviors started to be test, the mice were put in the experiment room for > 30 mins to adapt the environment. The equipment used in the behavioral tests was thoroughly cleaned with 75% alcohol before each mouse was tested. In the experiment recorded and analyzed by Ethovision XT software (Open field, Elevated plus maze, Barnes maze, the light and dark test, Novel object recognition), the experiment was recorded 1 s after the software recognized the mice. The center point of the mouse was considered to represent the localization of the mouse by the software. The same mouse finished all of the experiment. In all of the behavior, the mice were free-moving. The experiment was done between 13:00 to 18:00, which was in the dark phase of the light-dark cycle. In open field test, elevated plus maze, Barnes maze, light and dark test, the high light intensity (300 Lux) was used as aversive stimulation. In the three-chamber test and novel object recognition, the low light intensity (30 Lux) was used to video record. In the home cage video and fear conditioning test the video was record under infra-red.

2.17. Open field

Open field test was used to investigate the motor function and anxiety level of mice.

The mouse was put in the 45 cm × 45 cm box for free moving. The box was separated into 9 (3 × 3) equal size parts in the Ethovision XT software. The center part was used to be the center zone. The mice were put into the center zone. The behavior was recorded and analyzed by the software for 30 mins. The total distance and time that mouse spent in the center zone were exported by the software.

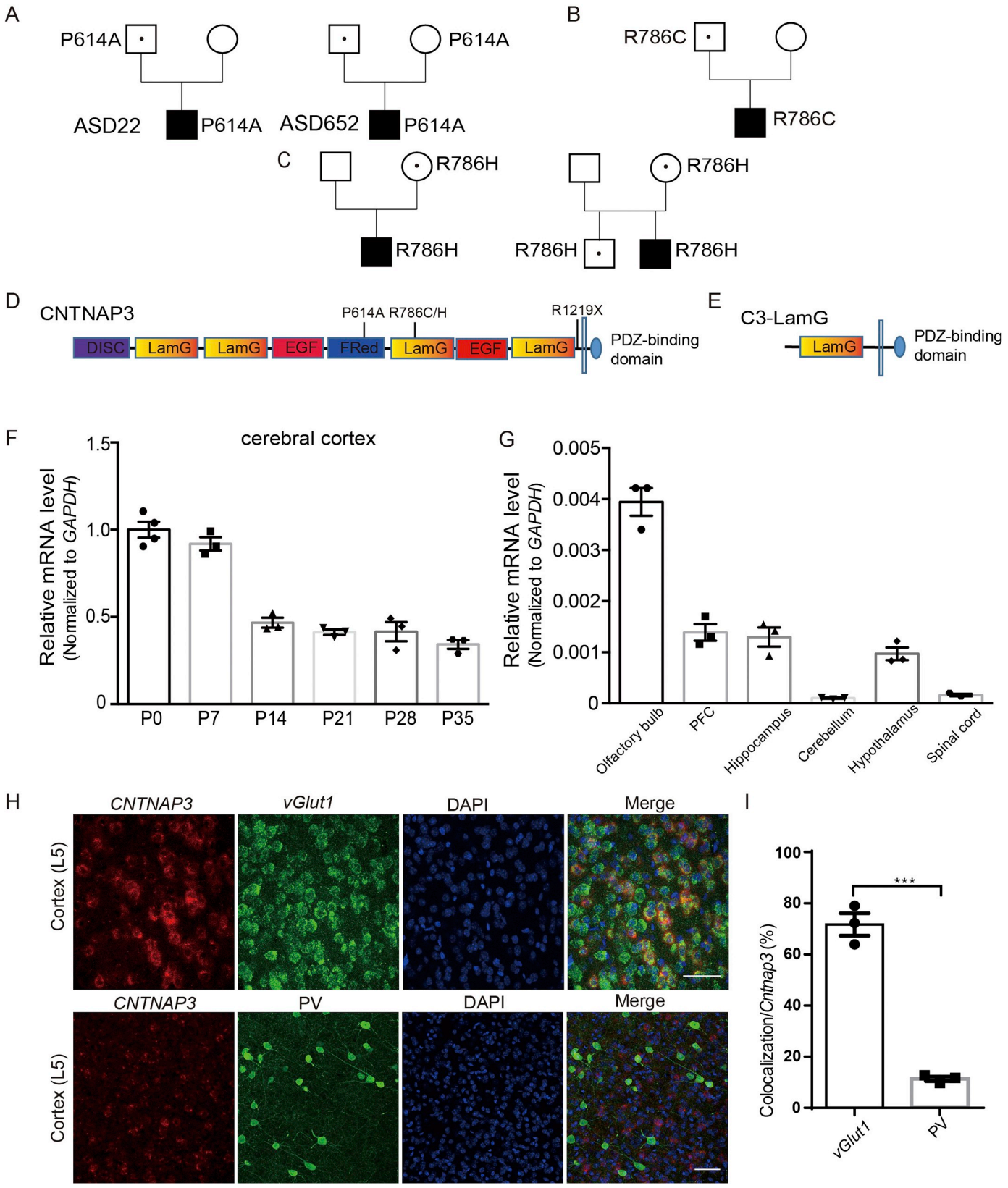

Fig. 1. ASD-related CNTNAP3 mutations and the expression pattern of Cntnap3 in the mouse brain.
(A) CNTNAP3 mutations found in the ASD patients. An inherited mutation of P614A was found in ASD22 and ASD652 trios. (B) Transmitted mutation of R786C was found in father and the proband. (C) Inherited mutations of R786H were found in SSC cases. (D) The schematic structure and locations of P614A, R786C/H and R1219X in the CNTNAP3 protein. (E) The schematic structure of CNTNAP3-LamG (C3-LamG for short). (F) Expression levels of *Cntnap3* in cerebral cortex of mouse in different ages (C57BL/6 J). (G) Expression levels of *Cntnap3* in different regions of the CNS of mouse (C57BL/6 J, Postnatal 28 days: P28). (H) Double labeling with immunostaining and *in situ* hybridization on P14 wild-type cortex with co-localization of *Cntnap3* (*in situ*, red) and *vGlut1* (*in situ*, green) or PV (immunostaining, green). (I) Mean percentage of co-localization of *Cntnap3* and *vGlut1* or PV (co-localization / *Cntnap3* positive). (F–H, mouse number $n = 3$ or 4 (Fig. 1 F P0), Scale bar: 50 μm.) Statistical significance was evaluated by Student's t-test: * $p < .05$, ** $p < .01$; error bars: ± SEM. See also Fig. S1.

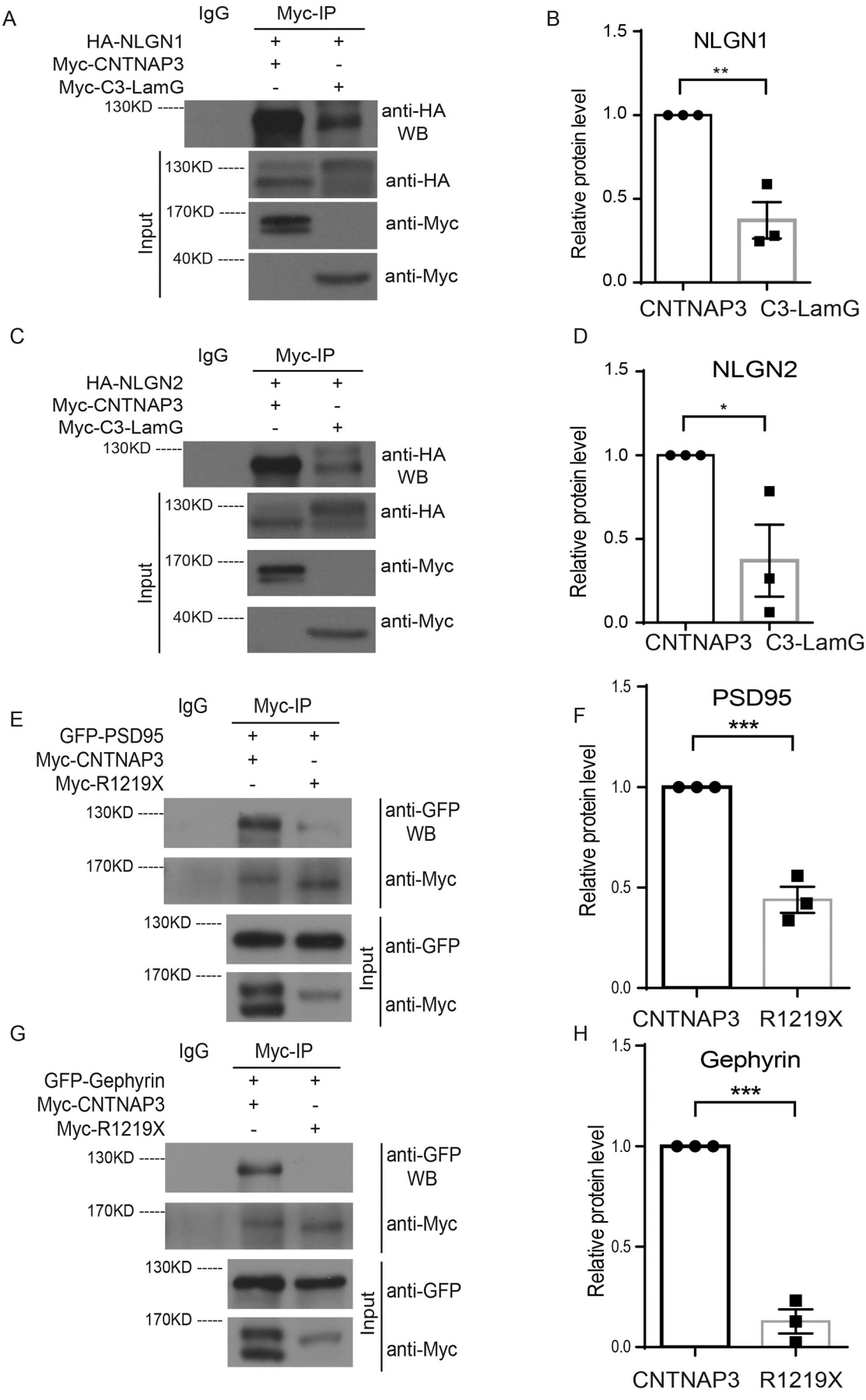

(caption on next page)

Fig. 2. The protein partner of CNTNAP3.
(A) Co-immunoprecipitation of myc-CNTNAP3, myc-C3-LamG and HA-NLGN1 in 293 T cells. Immunoprecipitated (IP) with anti-myc antibody, immunoblotted (IB) with anti-myc and anti-HA antibodies. (B) Quantitative analysis of HA-NLGN1 protein level interacts with myc-CNTNAP3 or myc-LamG. (C) Co-immunoprecipitation of myc-CNTNAP3, myc-C3-LamG and HA-NLGN2 in 293 T cells. IP with anti-myc antibody, IB with anti-myc and anti-HA antibodies. (D) Quantitative analysis of HA-NLGN2 protein level interacts with myc-CNTNAP3 or myc-LamG. (E) Co-immunoprecipitation of myc-CNTNAP3, myc-R1219X and GFP-PSD95 in 293 T cells. IP with anti-myc antibody, IB with anti-myc and anti-GFP antibodies. (F) Quantitative analysis of GFP-PSD95 protein level interacts with myc-CNTNAP3 or myc-R1219X. (G) Co-immunoprecipitation of myc-CNTNAP3, myc-R1219X and GFP-Gephyrin in 293 T cells. IP with anti-myc antibody, IB with anti-myc and anti-GFP antibodies. (H) Quantitative analysis of GFP-Gephyrin protein level interacts with myc-CNTNAP3 or myc-R1219X. (B, D, F, H, n number = 3 independent biological repeat) Statistical significance was evaluated by Student's t-test: * $p < 0.05$, ** $p < 0.01$; error bars: ± SEM. See also Fig. S2.

2.18. Elevated plus maze

Elevated plus maze was used to investigate anxiety level of mice.

The elevated plus maze had 2 open arms (30 cm × 6 cm), 2 close arms (30 cm × 6 cm) and the center part (6 cm × 6 cm). The same arms were on the opposite site of center part. The mouse was placed in the center part of the maze with its head to the same close arm to start the experiment. The elevated plus maze test was recorded and analyzed by the software for 10 mins. The time that mouse spent in the open arms or close arms was exported by the software.

2.19. Three-chamber test

Three-chamber test was used to investigate the social behavior of mice.

The box (60 cm × 45 cm) with 3 chambers was used in the test. The experiment was divided into 3 parts. For each part, the mouse was put into the center chamber; the test was recorded and analyzed by the software for 10 mins. For the first part, the cages (10 cm × 5 cm) were empty in both sides of the right or left chambers. For the second part, one stranger WT C57BL/6 J mouse was put in one random cage, the other cage was empty. For the last part, another stranger WT C57BL/6 J mouse was added to the leftover empty cage. The area 8 cm around the cage was considered to be the interaction zone (Fig. S5 A and B). The three-chamber test was recorded and analyzed by the software for 10 mins in each part. The latency time between 2 parts was 5 mins for adding the mouse. The time that mouse spent in the interaction zone was exported by the software.

2.20. Barnes maze

Barnes maze was used to investigate the spatial learning and memory of mice.

A 1.5 m diameter disc with 40 holes was used in the experiment and the highly light was used to be the aversive stimulation. The experiment was divided into 2 parts: spatial acquisition (from day 1 to day 4) and reference memory (day 5 and day 12). In the spatial acquisition part, placed the mouse in the middle of the maze and allowed the mouse explore the maze for 3 min. During these 3 min number errors and primary latency time were measured by the experimenter. The trial would end when the mouse entered the goal tunnel or after 3 min had elapsed. Immediately after the mouse entered the tunnel, the mouse was allowed to stay in the tunnel (dark area) for 1 min. If the mouse did not reach the goal within 3 min the experimenter should guide the mouse gently to the escape box and left the mouse inside for 1 min. The latency time were measured as 180 s. Placed the mouse in its home cage, cleaned and rotated the maze until the next trial. All of the mice would receive 4 trials per day with an inter-trial interval of 15 min during 4 days. In the reference memory part, on day 5 and day 12, the target hole must be closed. Placed the mouse in the middle of the maze and allowed the mouse explore the maze for 90 s. Removed the mouse after a fixed interval (90 s), numbers of errors and latency time to reach the virtually target hole were measured. The time mice spent in different quadrant was analyzed by Ethovision XT software.

2.21. The light and dark test

The light and dark test was used to investigate anxiety level of mice.

The box (45 cm × 30 cm) with 2 chambers was used in the test; the dark part (15 cm × 30 cm) was covered with a black plate and linked with the light box (30 cm × 30 cm) with an opened gate (5 cm × 5 cm). The box was put under the highly light. The mouse was put into the dark box and started the test. The light and dark test was recorded and analyzed by the software for 10 mins. The time that mouse spent in the light box was exported by the software.

2.22. Novel object recognition

Novel object recognition was used to investigate the mice's object recognition function and to test the specific features of memory (recognition memory: the shape and color of the toys).

The experiment was done in the box of three-chamber test. The experiment was divided into 2 phases: the recognition part and novel object recognition part. In the recognition part two toys (both gray cylinder, bottom diameter: 6 cm; height: 8 cm) were put in the different chambers (the same position we place the cage in the three-chamber test). The mouse was put into the center chamber. The novel object recognition phase was one hour after the recognition phase. One of the toys was changed for a novel toy (white cuboid: 6 cm × 6 cm × 8 cm) in the same position. The area within 8 cm around the toy was considered to be the recognition zone. The novel object recognition test was recorded and analyzed by the software for 10 mins. The time that mouse spent in the recognition zone was calculated by the software.

2.23. Fear conditioning test

Fear conditioning test was used to investigate the fear memory of mice.

One day before fear conditioning, placed the mouse in the training context box for 10 min to allow habituation to the context. The next day, placed the mouse to the context for 10 min and then give the mouse with 3 trials 2 s, 0.8 mA shock with the cue of sound, the latency between the trials was 2 mins. Moved the mouse to its home cage. The next day, placed the mouse in the context box for 5 mins and recorded the freeze percentage. 1 h later, placed the mouse again to the context with a raster paper inside the context box. The cue started 5 mins later without shock. The freeze percentage in the 3 mins before the 2 s was used to be the adjustment freeze percentage, the freeze percentage in the 3 mins after the cue was used to be the cue-test freeze percentage. In the fear extinction experiment, 10 trials of 2 s cue without shock were given; the latency time between the trials was 2 mins. The freeze percentage in the 2 mins after the cue was used as the extinction freeze percentage.

2.24. Home cage video

Home cage video was used to investigate the repetitive behavior of mice.

The mouse was put in the home cage 2 days in the experiment room before the video started. The experiments were in the normal circadian rhythms (12 h light and 12 h dark) in both experiment room and video

recorded box. The video was recorded for 24 h. The grooming and digging time that mice spent in the first half hour after turn off the light and the half hour 6 h after turn off the light were counted by the experimenter that do not know the genotype of the mice.

The order of the behavioral tests for *Cntnap3*$^{-/-}$ mice was Open field test, Three-chamber test, Elevated plus maze, Novel object recognition, The light and dark test, Barnes maze, Home cage video and Fear conditioning test. The order of the behavioral tests for *Cntnap3* conditional knockout mice was Open field test, Three-chamber test, Elevated plus maze and Barnes maze. When one behavioral test was finished, the next behavioral test would be started 2 days after the behavioral test before.

2.25. Statistical analysis

Statistical tests were carried out using GraphPad Prism 6 (Graphpad Software, lnc., RRID:SCR_002798). Two-tailed Student's *t*-test was used for sample pairs, one-way ANOVA followed by Tukey's multiple comparison tests was used for 3 or more conditions, two-way ANOVA was used for the curve (Barnes maze and fear extinction). For three-chamber test, paired t-test was used. Data distribution was test by Kolmogorov-Smirnov test and Shapiro-Wilk test by SPSS software (IBM, RRID:SCR_002865). The data distribution was normal distribution. Results were shown as mean ± SEM, and "n" represented to either the number of neurons (for morphological analysis and electrophysiology), the number of animals (for qPCR, *in situ* hybridization and behavioral tests), repeat experiment (for western blot). All of the mice used in the morphological analysis were at least 3 from 2 different litters. The *in vitro* experiments were done at least 3 times independently. All data analyses were performed blinded to the experimental condition. All conditions statistically different from control are indicated. * $P < .05$; ** $P < .01$; *** $P < .001$.

Exclusion criteria: If the data was not in the 95% confidence interval of the group, the data would be excluded. In all of the experiment, especially behavioral test, if the mice were not healthy, for example, without beard, the mice would not be used in the experiment.

3. Results

3.1. Identification of CNTNAP3 mutations in ASD patients and the expression pattern of Cntnap3 in the mouse brain

In the whole-exome sequencing study of 120 ASD patients collected from Shanghai Mental Health Hospital (Wen et al., 2017), we found two probands (ASD22, ASD652) carrying the same inherited mutation (causing amino acid alternation P614A) in the *CNTNAP3* gene, validated by Sanger sequencing (Fig. 1A, D, Fig. S1 A, B). We identified another proband featured "Human phenotype ontology (HPO): autism" in the database of brain disorders patients in Fudan Children's Hospital of Shanghai, in which an inherited mutation (R786C) transmitted from the father in the *CNTNAP3* gene, suggesting the connection between *CNTNAP3* and ASD (Fig. 1B, D, Fig. S1 C).

In order to determine whether *CNTNAP3* mutations exist in ASD populations from different geographic regions, we next searched the Simons simplex collections (SSC) and found 2 ASD probands carrying R786H mutation in the *CNTNAP3* gene, among 2600 ASD trios, both of which are inherited from unaffected mothers (Fig. 1C, D). In conclusion, there are 5 mutations of CNTNAP3 (G410S, P614A, R786C/H, R1219X) which were reported to be found in ASD patients yet, which caused 4 amino acid changed and one stop-gain *de novo* mutation (Turner et al., 2017; Vaags et al., 2012). We further examined the mutation rates of *CNTNAP3* mutations (G410S, P614A, R786C, R786H and R1219X) in the gnomAD database (http://gnomad.broadinstitute.org). P614A, R786C and R1219X exhibited extremely low occurrence (< 0.01%) in total 245,686 populations of the gnomAD database, indicating that they are rare variants. The R786H mutation occurs 0.012% in gnomAD database, which is still much lower than it in SSC (2/2600, 0.077%), suggesting the possible enrichment of R786H mutation in ASD cohorts. However, G410S exhibited high occurrence (3.7%) in total 276,826 populations of the gnomAD database, indicating that G410S may be just a single-nucleotide polymorphism. The R786 locates in the LamG domains, P614 is within fibrinogen-related (FRed) domain, and R1219 locates in the link region before trans member domain (Fig. 1D).

To investigate the role of CNTNAP3 in brain development, we first examined the expression profile of CNTNAP3 in developmental stages and various regions in the mouse brain *via* quantitative PCR (Fig. 1F, G, Fig. S1 D, E, n number = 3 or 4 mice for each group), due to lack of the suitable antibody against the mouse CNTNAP protein. We found that CNTNAP3 was highly expressed in cortex and hippocampus of the mouse postnatal brain (Fig. 1F, G, Fig. S1 D) and had relative low expression level in cerebellum and spinal cord (Fig. 1G). We further performed *in situ* hybridization using probes against the mouse *Cntnap3* mRNA together with immunostaining with various cell markers in cortex and hippocampus to characterize the expression pattern of CNTNAP3 in different neuronal cell types (Fig. 1H, Fig. S1F, n number = 3 mice for either group). Interestingly, we found that the majority (~70%) of CNTNAP3-expressing neurons were co-localized with vesicular glutamate transporter 1 (vGlut1) in cerebral cortex, whereas around 10% CNTNAP3-expressing neurons are parvalbumin (PV)-positive, indicating that CNTNAP3 is mainly expressed in glutamatergic neurons in cortex (Fig. 1I, n number = 3 mice for either group, Student's *t*-test, $p = 0.0002$).

3.2. CNTNAP3 interacts with NLGNs and NRXNs

CNTNAP3 has repeated LamG domains and EGF domains, as well as an intracellular PDZ-binding domain, which was structurally similar with NRXN superfamily proteins (Fig. 1D). Hence, we would like to determine whether CNTNAP3 interacted with synaptic adhesion molecules, such as Neuroligin1 (NLGN1), Neuroligin 2 (NLGN2) and synaptic scaffolding proteins. We constructed a plasmid expressing hemagglutinin (HA)-tagged full-length human CNTNAP3. To address which domain would be responsible for the interaction, we also made the plasmid expressing only one extracellular LamG domain and the intracellular PDZ-binding domain of CNTNAP3 protein (C3-LamG) (from Phe1046 to Cys1288, Fig. 1E).

By the co-immunoprecipitation experiment, we found the CNTNAP3 interacted with both NLGN1 and NLGN2 (Fig. 2A, C). Deletion of extracellular LamG domains (C3-LamG) significantly weaken, but not blocked the interaction, indicating that only one LamG domain was sufficient for the interaction between CNTNAP3 and NLGN1 or NLGN2 (Fig. 2A–D, n number = 3 independent biological repeats, Student's *t*-test, Fig. 2 B: $p = 0.0044$, Fig. 2 D: $p = 0.0429$). CNTNAP3 also interacted with synaptic scaffolding proteins, including PSD-95 and Gephyrin but not SHANK3 (Fig. 2E, G, Fig. S2 A). NLGN1 and PSD-95 primarily located in the post-synaptic compartment of excitatory synapse, whereas NLGN2 and Gephyrin localized in the inhibitory synapses, these evidences suggest that CNTNAP3 may exist in both excitatory and inhibitory synapses.

Among the 5 mutations, R1219X has almost all of the extracellular region but not trans member region or PDZ-binding domain. We presumed that R1219X could not interact with PSD-95 or Gephyrin because of the absent of PDZ-binding domain (Fig. 2F, H n number = 3 independent biological repeats, Student's t-test, Fig. 2F: $p = 0.0010$, Fig. 2H: $p = 0.0001$), which suggested R1219X may be a *loss of function* mutation with the disability of recruiting scaffolding proteins.

3.3. CNTNAP3 regulates excitatory and inhibitory synapse development differentially

To assess the function of CNTNAP3 in synaptic development, we

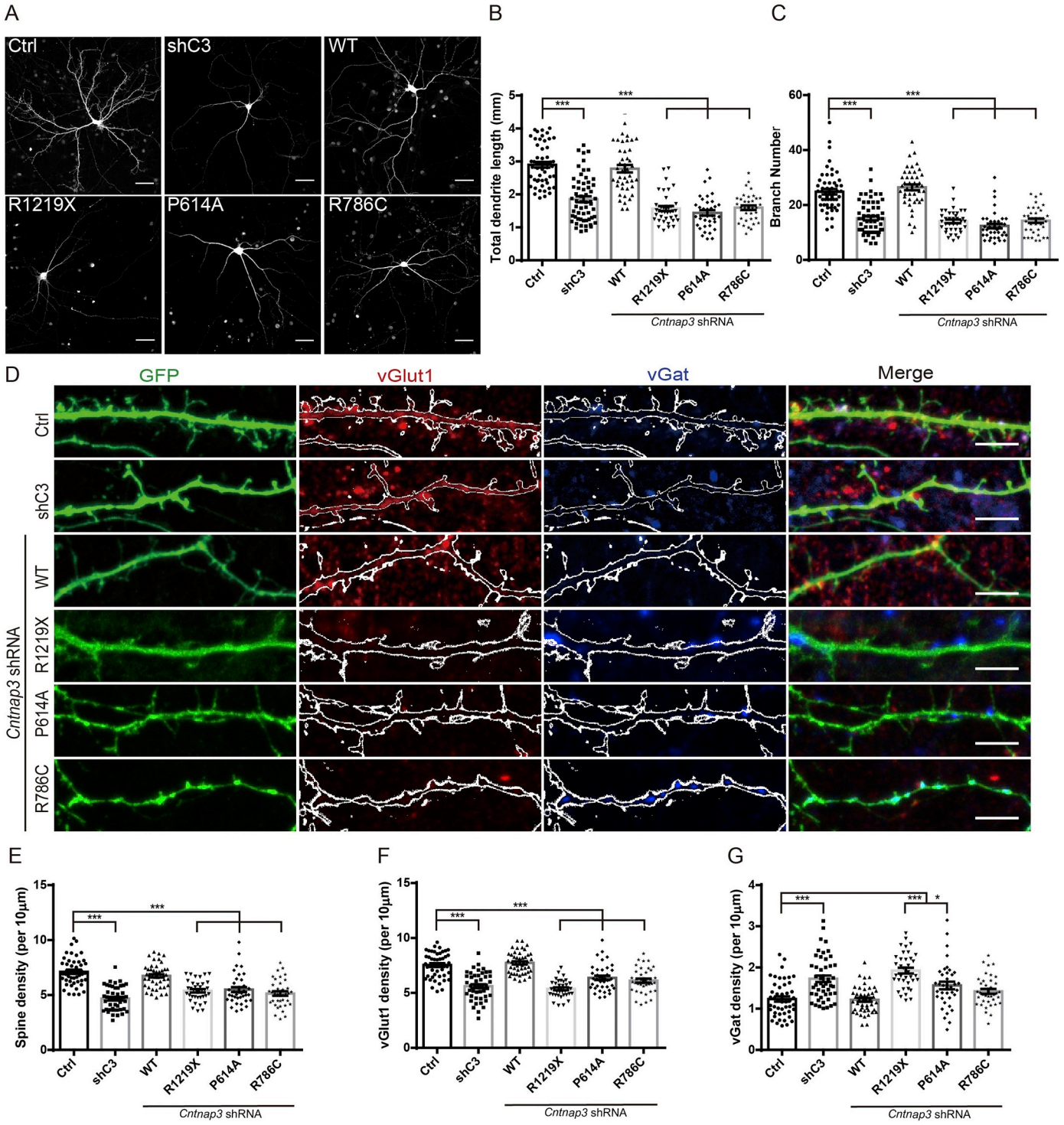

Fig. 3. CNTNAP3 regulated neurite and synapse development.
(A) Immunostaining of GFP in cultured E13.5 cortex neurons. (E13.5 + DIV 14, Scale bar: 50 μm) (B) Dendritic length analysis of (A). (Counted neuron numbers Ctrl: $n = 54$, shC3: $n = 58$, WT: $n = 43$, R1219X: $n = 37$, P614A: $n = 36$, R786C: $n = 36$.) (C) Branch numbers analysis in (A). (D) Immunostaining of GFP (green), vGlut1 (red) and vGat (blue) in cultured E13.5 cortex neurons. (E13.5 + DIV 14, counted neuron numbers Ctrl: $n = 47$, shC3: n = 47, WT: n = 47, R1219X: $n = 37$, P614A: n = 37 R786C: $n = 37$. Scale bar: 5 μm) (E) Quantitative analysis of spine density in (D). (F) Quantitative analysis of vGlut1 density in (D). (G) Quantitative analysis of vGat density in (D). Statistical significance was evaluated by one-way ANOVA: $^{*}p < 0.05$, $^{**}p < 0.01$, $^{***}p < 0.001$. Error bars: ± SEM. See also Fig. S3.

constructed a short hairpin RNA (shRNA) against the mouse *Cntnap3* mRNA and confirmed the efficiency of down-regulating the endogenous expression level of *Cntnap3* (Fig. S2 B, n number = 3 independent biological repeats, Student's t-test, $p < 0.0001$). We next investigated whether the knockdown of *Cntnap3* could affect neuronal morphology and synaptic development in cultured mouse primary neurons. We transfected GFP expressing plasmids, together with control vector, *Cntnap3* shRNA, human WT *CNTNAP3* cDNA as well as human *CNTNAP3* cDNA carrying ASD-related mutations, respectively to the cultured neurons. Since mouse *Cntnap3* shRNA does not target human *CNTNAP3*, human WT *CNTNAP3* cDNA could serve as a rescue construct for shRNA knockdown. We found that knockdown of CNTNAP3

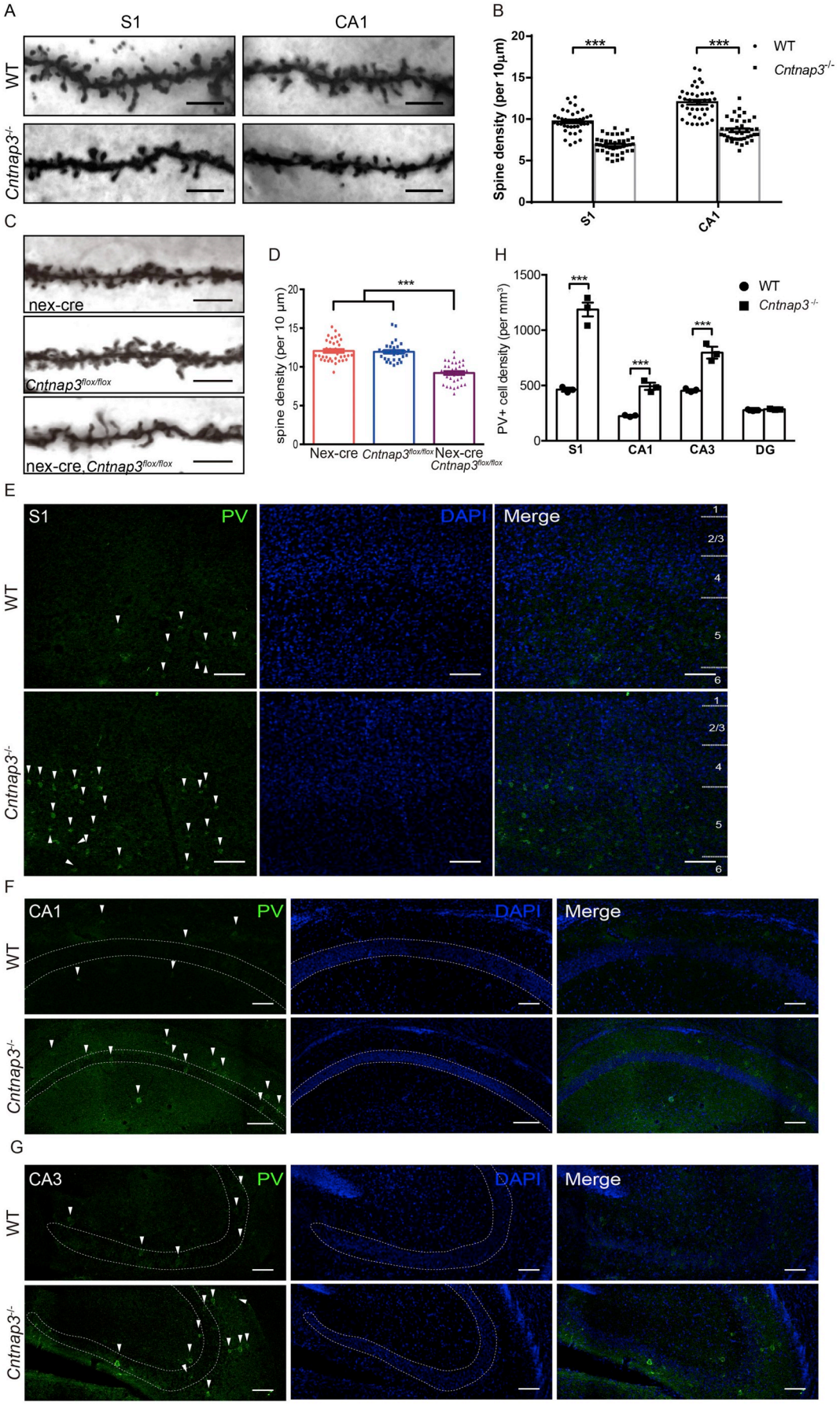

(caption on next page)

Fig. 4. *Cntnap3*$^{-/-}$ mice showed decreased spine density and increased PV-positive neurons in cortex and hippocampus.
(A) Golgi staining in adult *Cntnap3*$^{-/-}$ mice in S1 (primary somatosensory cortex) and CA1 region. (apical dendrite, 2–4 months of age, mice number n = 3 for either WT or *Cntnap3*$^{-/-}$, scale bar: 5 μm) (B) Quantitative analysis of spine density in *Cntnap3*$^{-/-}$ mice. (neuron numbers, WT: $n = 40$, *Cntnap3*$^{-/-}$: n = 40 for both S1 and CA1 region) (C) Golgi staining in adult *Nex-Cre:Cntnap3*$^{flox/flox}$ mice in CA1 region. (apical dendrite, from 2 to 4 months of age, mice number n = 3 for each genotype, scale bar: 5 μm) (D) Quantitative analysis of spine density in *Nex-Cre:Cntnap3*$^{flox/flox}$ mice. (neuron numbers *Nex-Cre*: n = 36, *Cntnap3*$^{flox/flox}$: $n = 30$, *Nex-Cre:Cntnap3*$^{flox/flox}$: $n = 34$, mice number n = 3 for each genotype) (E) Immunochemistry of PV (green) in S1 region of *Cntnap3* KO mice at postnatal 14 days of age (P14). (Scale bar: 100 μm) (F) Immunochemistry of PV (green) in hippocampus CA1 region of P14 *Cntnap3*$^{-/-}$ mice. (Scale bar: 100 μm) (G) Immunochemistry of PV (green) in hippocampus CA3 region of P14 *Cntnap3*$^{-/-}$ mice. (Scale bar: 100 μm) (H)Quantitative analysis of density of PV positive neurons in *Cntnap3*$^{-/-}$ mice. (mice number, n = 3 for WT and KO). Statistical significance was evaluated by Student's *t*-test (*Cntnap3*$^{-/-}$ *vs.* WT) or one-way ANOVA (*Nex-Cre:Cntnap3*$^{flox/flox}$ *vs.* other groups): ***$p < 0.001$. Error bars: ± SEM. See also Fig. S4.

expression led to significantly decrease of axonal and dendritic length, as well as dendritic branch number (Fig. 3A–C, Fig. S3, n number represent for neuron number, see figure legend, 3 independent biological repeats, one-way ANOVA, ***: $p < 0.001$). It is worth noting that although human WT *CNTNAP3* cDNA was able to fully restore axonal and dendritic length to normal level after shRNA knockdown, three ASD-related mutations (R1219X, P614A and R786C) were not able to rescue defects caused by *Cntnap3* shRNA, exhibiting *loss-of-function* effects (Fig. 3B, C, Fig. S3 B, D).

Next, we would like to investigate whether CNTNAP3 contributed to synaptic development. After transfection of GFP expressing plasmids, along with vector control, or *Cntnap3* shRNA, as well as *Cntnap3* shRNA with human WT *CNTNAP3* or ASD-related mutations, respectively in mouse primary cortical neurons *in vitro* for 14 days, we then measured amounts of excitatory synapses by anti-vesicular glutamate transporter 1 (vGlut1) immunostaining and numbers of inhibitory synapses by anti-vesicular GABA transporter (vGat) immunostaining onto the GFP-expressing neurons transfected with either control vectors or various manipulations (Fig. 3D). We found that knockdown of *Cntnap3* led to decrease of excitatory synapse formation which were fully rescued by WT CNTNAP3, but not the R1219X, P614A and R786C mutants (Fig. 3D, F n number represent for neuron number, see figure legend, 3 independent biological repeats, one-way ANOVA, ***: $p < 0.001$). Interestingly, inhibitory synapse numbers measured by anti-vGat staining were increased after knockdown of CNTNAP3, which could be fully rescued to normal level by WT and R786C, but not R1219X nor P614A mutant, suggesting that CNTNAP3 may play a negative role in repressing formation of inhibitory synapse and R1219X, P614A may exhibit *loss-of-function* effects in this regard (Fig. 3D, G). Furthermore, numbers of spine were also markedly decreased in the CNTNAP3 knockdown group, which were restored to the normal level when co-expressed with WT CNTNAP3, but not R1219X, P614A nor R786C mutants (Fig. 3D, E). These evidences indicate that CNTNAP3 may promote excitatory glutamatergic synapse formation, whereas inhibit GABAergic synapse formation. Additionally, ASD-related mutations may exhibit *loss-of-function* effects regarding to excitatory and inhibitory synapses formation specifically.

3.4. CNTNAP3 regulates development of excitatory synapse and PV-positive inhibitory neurons in vivo

To address the role of CNTNAP3 *in vivo*, we constructed *Cntnap3*$^{-/-}$ mouse by CRISPR/Cas9 technology and conditional knockout of *Cntnap3* mouse by flanking exon 3 with LoxP cassettes with homology recombination strategy (Fig. S2 C, D). We first examined whether development of excitatory synapses can be altered in *Cntnap3*$^{-/-}$ mice by measuring the morphology of dendritic spine of pyramidal neurons in hippocampal CA1 and S1 (primary somatosensory cortex) region. Golgi staining showed that spine density of hippocampal CA1 and S1 neurons significantly decreased in *Cntnap3*$^{-/-}$ mice in comparison with WT mice, suggesting that CNTNAP3 plays a critical role in excitatory synapse development *in vivo* (Fig. 4 A, B n number represent for neuron number, see figure legend, 3 mice, Student's *t*-test, $p < 0.0001$). Next, we crossed *Nex-Cre* mice with *Cntnap3*$^{flox/flox}$ mice to specifically delete *Cntnap3* in excitatory neurons(Kashani et al., 2006). In *Nex-Cre:Cntnap3*$^{flox/flox}$ mice, spine density also dramatically decreased in hippocampal CA1 neurons comparing to control mice, indicating that CNTNAP3 likely regulates development of excitatory synapse through cell-autonomous manner (Fig. 4C, D, n number represent for neuron number, see figure legend, 3 mice, one-way ANOVA, ***: $p < 0.001$).

Strikingly, we found that parvalbumin-positive GABAergic neurons markedly increased in cortical regions and hippocampus of *Cntnap3*$^{-/-}$ mice in comparison with WT mice (Fig. 4 *E*-H, Fig. S4 A, n number = 3 mice for either group, Student's *t*-test, ***: $p < 0.001$). But somatostatin (SST)-positive GABAergic neurons remained unaffected in *Cntnap3*$^{-/-}$ mice (Fig. S4 B–F, n number = 3 mice for either group, Student's t-test). These data suggest that CNTNAP3 may specifically hamper development of PV-positive subtype of GABAergic neurons.

3.5. CNTNAP3 regulates excitatory and inhibitory synaptic transmission in vitro

To determine the role of CNTNAP3 in synaptic transmission *in vitro*, the whole-cell patch clamp recording was performed on the hippocampal CA1 neurons and layer 5 neurons of neocortex in acute slice preparations of *Cntnap3*$^{-/-}$ mice and WT mice as control (Fig. 5A). We firstly measured passive electrical properties of these cells, including resting membrane potential (RMP), input resistance (R_{in}) and membrane capacity (Cm) (Fig. 5B–D). Our results showed that intrinsic properties of neurons in layer 5 of *Cntnap3*$^{-/-}$ mice were equivalent to their counterparts in control mice (The upper panel of Fig. 5B–D). The measured membrane constant indicated that the deletion of *Cntnap3* did not harm the maturation of neurons in cortex. However, hippocampal CA1 pyramidal neurons of *Cntnap3*$^{-/-}$ mice appeared more depolarized compared to the cells in WT mice (The lower panel of Fig. 5B, WT $n = 39$ cells/4 mice, *Cntnap3*$^{-/-}$ $n = 40$ cells/4 mice, Student's *t*-test, $p = 0.0001$), while the resting membrane potential appeared significantly higher in mutant mice. Moreover, the R_{in} was elevated and the Cm decreased in *Cntnap3*$^{-/-}$ mice comparing to WT mice (The lower panel of Fig. 5 C, D, Fig. 5C, WT n = 39 cells/4 mice, *Cntnap3*$^{-/-}$ n = 40 cells/4 mice, Student's *t*-test, $p < 0.0001$, Fig. 5 D, WT n = 39 cells/4 mice, *Cntnap3*$^{-/-}$ n = 40 cells/4 mice, Student's t-test, $p < 0.0001$), also indicating that the pyramidal neurons in CA1 of mutant mice were less mature than those of the control neurons. These results suggest that membrane properties and ion channel distributions may be altered in hippocampal CA1 neurons in *Cntnap3*$^{-/-}$, in the absence of *Cntnap3*. These changes of process of maturation would induce the morphological changes in neurons in *Cntnap3*$^{-/-}$ mice mentioned before.

These developmental changes may further shape properties of action potentials and membrane activities. We thus investigated the inward and outward current during the excitation of neurons evoked by a series of voltage pulses in cortical layer 5 and hippocampal CA1 neurons of *Cntnap3*$^{-/-}$ and WT mice (Fig. 5E). We found that amplitude of inward currents of both layer 5 and CA1 neurons significantly decreased in *Cntnap3*$^{-/-}$ mice compared to those in WT mice (Fig. 5F, layer 5: WT $n = 29$ cells/4 mice, *Cntnap3*$^{-/-}$ $n = 22$ cells/4 mice Two-way ANOVA, $p = 0.0001$, CA1: WT n = 39 cells/4 mice, *Cntnap3*$^{-/-}$ n = 40 cells/4 mice, Two-way ANOVA, $p = 0.0033$). The outward currents displayed the same tendency (Fig. 5G, layer 5: WT n = 29

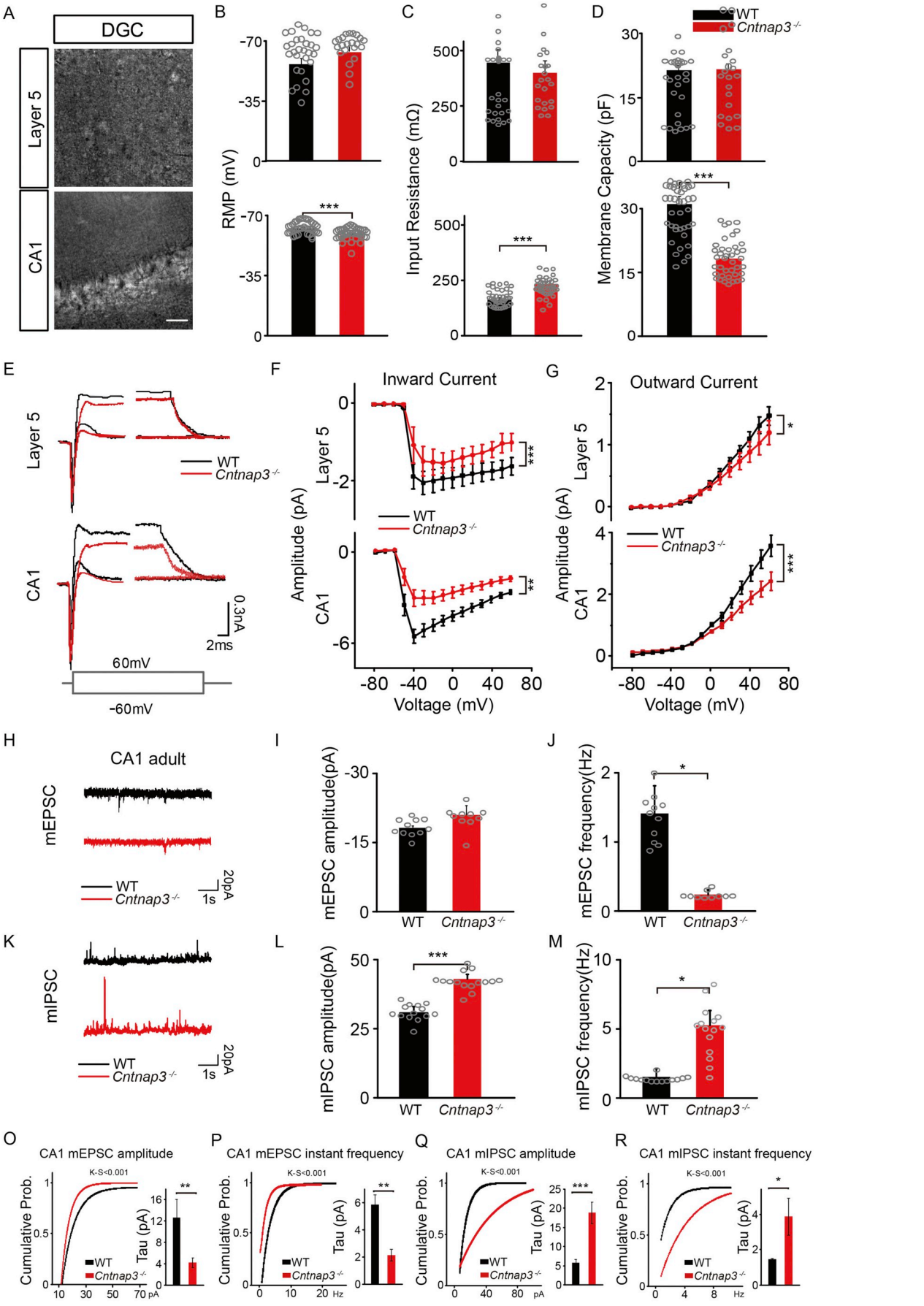

(caption on next page)

Fig. 5. *Cntnap3*$^{-/-}$ mice exhibited decreased mEPSC and increased mIPSC frequency in hippocampal CA1 neurons.
(A) Images of whole-cell recording of cortical layer 5 and hippocampal CA1 neurons in bright field, scale bars: 50 μm. Resting membrane potential (B), input resistance (C) and membrane capacity (D) of neurons in cortical layer 5 (upper panel, 29 cells from 4 WT mice, 22 cells from 4 KO mice) and hippocampal CA1 (lower panel, 39 cells from 4 WT mice, 40 cells from 4 KO mice). (E) Representative current responses of neurons in cortical layer 5 and hippocampal CA1 at -60 mV and 60 mV. Amplitude of inward current (F) and outward current (G) responses of neurons in cortical layer 5 (upper panel, inward current: 29 cells from 4 WT mice, 22 cells from 4 KO mice, outward current: 29 cells from 4 WT mice, 22 cells from 4 KO mice) and hippocampal CA1 (lower panel, inward current: 39 cells from 4 WT mice, 40 cells from 4 KO mice, outward current: 39 cells from 4 mice, 40 cells from 4 KO mice) evoked by a series of voltage steps. (H) Representative mEPSC traces of neurons of hippocampal CA1 in *Cntnap3*$^{-/-}$ and WT adult mice. Amplitude (I) and frequency (J) of mEPSC of hippocampal CA1 in KO and WT adult mice (11 cells from 5 WT mice, 10 cells from 5 KO mice). (K) Representative mIPSC traces of neurons of hippocampal CA1 in KO and WT adult mice. Amplitude (L) and frequency (M) of mIPSC of hippocampal CA1 in KO and WT adult mice (14 cells from 5 WT mice, 15 cells from 5 KO mice). Cumulative distributions and tau of CA1 adult mEPSC amplitude (O), mEPSC instant frequency (P), CA1 adult mIPSC amplitude (Q) and mEPSC instant frequency (R).
Statistical significance was evaluated by Student's *t*-test or two-way ANOVA (curve): * $p < 0.05$; ** $p < 0.01$; *** $p < 0.001$. Error bars: ± SEM. See also Fig. S5.

cells/4 mice, *Cntnap3*$^{-/-}$ n = 22 cells/4 mice Two-way ANOVA, $p = 0.0470$, CA1: WT n = 39 cells/4 mice, *Cntnap3*$^{-/-}$ n = 40 cells/4 mice, Two-way ANOVA, $p = 0.0005$). These results suggested that knockout of *Cntnap3* altered excitability of both cortical and hippocampal neurons. However, when we measured firing rate and amplitude of action potentials of cortical layer 5 and hippocampal CA1 neurons (Fig. S5 A-C, WT n = 39 cells/4 mice, *Cntnap3*$^{-/-}$ n = 40 cells/4 mice), we found that these properties were not influenced by knockout of *Cntnap3* (Fig. S5 *E*-J, WT n = 39 cells/4 mice, *Cntnap3*$^{-/-}$ n = 40 cells/4 mice). We reasoned that the altered excitability did not lead to change of fire rate might be due to the input of these neurons were also changed in the absence of *Cntnap3*. This result indicated that the Cntnap3 deletion disrupted the membrane ion channels (especially Na and K ion channel) of neurons in cortex and CA1, and weakened the inward and outward current of neurons of mutant mice. But the deletion did not influence on the level of intracellular calcium and chlorine, which were directly related to APs firing rate of neurons.

Therefore, to elucidate the role of CNTNAP3 in synapse development, we further examined excitatory and inhibitory synaptic transmission in the hippocampal CA1 region of *Cntnap3*$^{-/-}$ mice. We measured miniature excitatory postsynaptic currents (mEPSC) and miniature inhibitory postsynaptic current (mIPSC) in the presence of tetrodotoxin (TTX) in acute hippocampal slices of *Cntnap3*$^{-/-}$ and WT mice (Fig. S5 K, L, M). We found that the frequency, but not amplitude, of mEPSC significantly decreased in adult *Cntnap3*$^{-/-}$ mice, in consistent with the observation of decreased excitatory synapse development *in vitro* and reduced spine density *in vivo* (Fig. 5I, J, O, P, Fig. 5J: WT $n = 11$ cells/5 mice, *Cntnap3*$^{-/-}$ $n = 10$ cells/5 mice, Student's *t*-test, $p = 0.0489$, Fig. 5O: WT n = 11 cells/5 mice, *Cntnap3*$^{-/-}$ n = 10 cells/5 mice Curve: K–S test, $p = 9.79093*10^{-11}$, Histogram: Student's t-test, $p = 0.002134$, Fig. 5P : WT n = 11 cells/5 mice, *Cntnap3*$^{-/-}$ n = 10 cells/5 mice, Curve: K–S test, $p = 2.5706*10^{-8}$, Histogram: Student's *t*-test, $p = 0.00582$). Interestingly, both amplitude and frequency of mIPSC significantly increased in the hippocampal CA1 region of adult *Cntnap3*$^{-/-}$ mice, suggesting that numbers and strength of inhibitory synapses were both increased in *Cntnap3*$^{-/-}$ mice (Fig. 5L, M, Q, R, Fig. 5 L, WT $n = 14$ cells/5 mice, *Cntnap3*$^{-/-}$ $n = 15$ cells/5 mice Student's *t*-test, $p = 0.0004$, Fig. 5 M, WT n = 14 cells/5 mice, *Cntnap3*$^{-/-}$ n = 15 cells/5 mice Student's *t*-test, $p = 0.0275$, Fig. 5Q: WT n = 14 cells/5 mice, *Cntnap3*$^{-/-}$ n = 15 cells/5 mice, Curve: K–S test, $p = 3.8285*10^{-13}$, Histogram: Student's t-test, $p = 0.00095868$, Fig. 5 R: WT n = 14 cells/5 mice, *Cntnap3*$^{-/-}$ n = 15 cells/5 mice, Curve: K–S test, $p = 1.0717*10^{-10}$, Histogram: Student's t-test, $p = 0.01401$). We also measured mEPSC and mIPSC in adolescent mice from postnatal day 14 (P14) to 28 (P28). The frequency of mEPSC in *Cntnap3*$^{-/-}$ adolescent mice was significantly decreased (Fig. S5 N, O, Fig. S5 O, WT n = 10 cells/3 mice, *Cntnap3*$^{-/-}$ $n = 12$ cells/3 mice, Student's *t*-test, $p = 0.0019$), whereas the frequency of mIPSC was markedly increased (Fig. S5 P, Q, Fig. S5 Q, WT $n = 11$ cells/3 mice, *Cntnap3*$^{-/-}$ $n = 13$ cells/3 mice, Student's t-test, $p = 0.0499$). These results suggest that CNTNAP3 also plays a pivotal role in regulating excitatory and inhibitory synaptic transmission *in vitro*. Taken together, these evidences indicate that CNTNAP3 regulates intrinsic neuronal excitability, as well as playing an opposite role in controlling development of excitatory and inhibitory synapses.

3.6. Defects in social interaction, repetitive behaviors and cognition in *Cntnap3*$^{-/-}$ mice

Finally, we sought to determine whether deletion of *Cntnap3* may lead to autistic-like behavioral abnormalities in mouse, although previous studies showed that *Cntnap3* knockout mice exhibited the normal motor function and anxiety level(Hirata et al., 2016b). We performed a battery of behavioral tasks on *Cntnap3*$^{-/-}$, excitatory (*Nex-Cre: Cntnap3*$^{flox/flox}$) and inhibitory (*Vgat-ires-Cre: Cntnap3*$^{flox/flox}$) specific knockout mice. Remarkably, in the three-chamber test, *Cntnap3*$^{-/-}$ mice appeared no preference in staying with mouse over an empty cage, while still exhibited increased interaction time with novel mice over familiar mice, suggesting that *Cntnap3*$^{-/-}$ showed defects in social interactions (Fig. 6A, B, Fig. S6 A-C, $n = 12$ mice for either group, paired *t*-test: Fig. 6A: *Cntnap3*$^{-/-}$: $p = 0.2938$). Interestingly, we found that *Nex-Cre: Cntnap3*$^{flox/flox}$ mice, specific deletion of *Cntnap3* in excitatory neurons, showed no defects in recognizing either mice over cage, or novel over familiar mice (Fig. 6C, D, Fig. S7 A, $n = 11$ mice for each group, paired *t*-test). However, inhibitory neuron specific knockout mice, *Vgat-ires-Cre: Cntnap3*$^{flox/flox}$, exhibited defects in distinguishing novel mice with familiar mice, suggesting that *Cntnap3* in inhibitory neurons might contribute to social memory (Fig. 6E, F, Fig. S7 B, $n = 8$ mice for each group, paired *t*-test, Fig. 6F: *Vgat-ires-Cre: Cntnap3*$^{flox/flox}$: $p = 0.2242$).

Another phenotype of ASD patients is repetitive behaviors. Thus we measured the time which WT or *Cntnap3*$^{-/-}$ mice spent to groom or dig in one hour within its home cage. We found that *Cntnap3*$^{-/-}$ mice spent more time to self-groom or dig, which are considered to be repetitive behaviors (Fig. 6G, H, Extended Movie 1 and 2, n = 8 mice for either group, Student's *t*-test, Fig. 6G: $p = 0.0007$, Fig. 6H: $p = 0.0011$). These results suggest that *Cntnap3*$^{-/-}$ mice show the ASD-like behavior.

As the deletion of CNTNAP3 was found in one MR patient, we think that deletion of CNTNAP3 may lead to learning and memory disability, which is also an important accompanying phenotype of ASD. Next, we used the Barnes Maze test to examine whether *Cntnap3*$^{-/-}$ mice might have defects in learning and memory tasks. First, we found that *Cntnap3*$^{-/-}$ mice spent significantly longer time and explored more error holes to find the correct hole during the training session, suggesting that the learning ability in *Cntnap3*$^{-/-}$ mice was compromised (Fig. 6I, Fig. S6 D, $n = 12$ mice for either group, two-way ANOVA, Fig. 6I: $p = 0.0049$). We then performed the spatial and long-term spatial memory tasks at day 5 and day 12 after training, respectively. We found that *Cntnap3*$^{-/-}$ mice spent markedly increased latency time and explored more error holes in both memory tests, indicating the both spatial and long-term spatial memory capacity of *Cntnap3*$^{-/-}$ mice were severely affected (Fig. 6J–M, Fig. S6 E, n = 12 mice for either group, Student's *t*-test, Fig. 6J: $p = 0.0022$, Fig. 6 K: $p = 0.0158$, Fig. 6 L: $p = 0.0306$, Fig. 6M: $p = 0.0304$, Fig. S6 E: $p = 0.0026$). We found no defects of *Cntnap3*$^{-/-}$ mice in consequent series of tests,

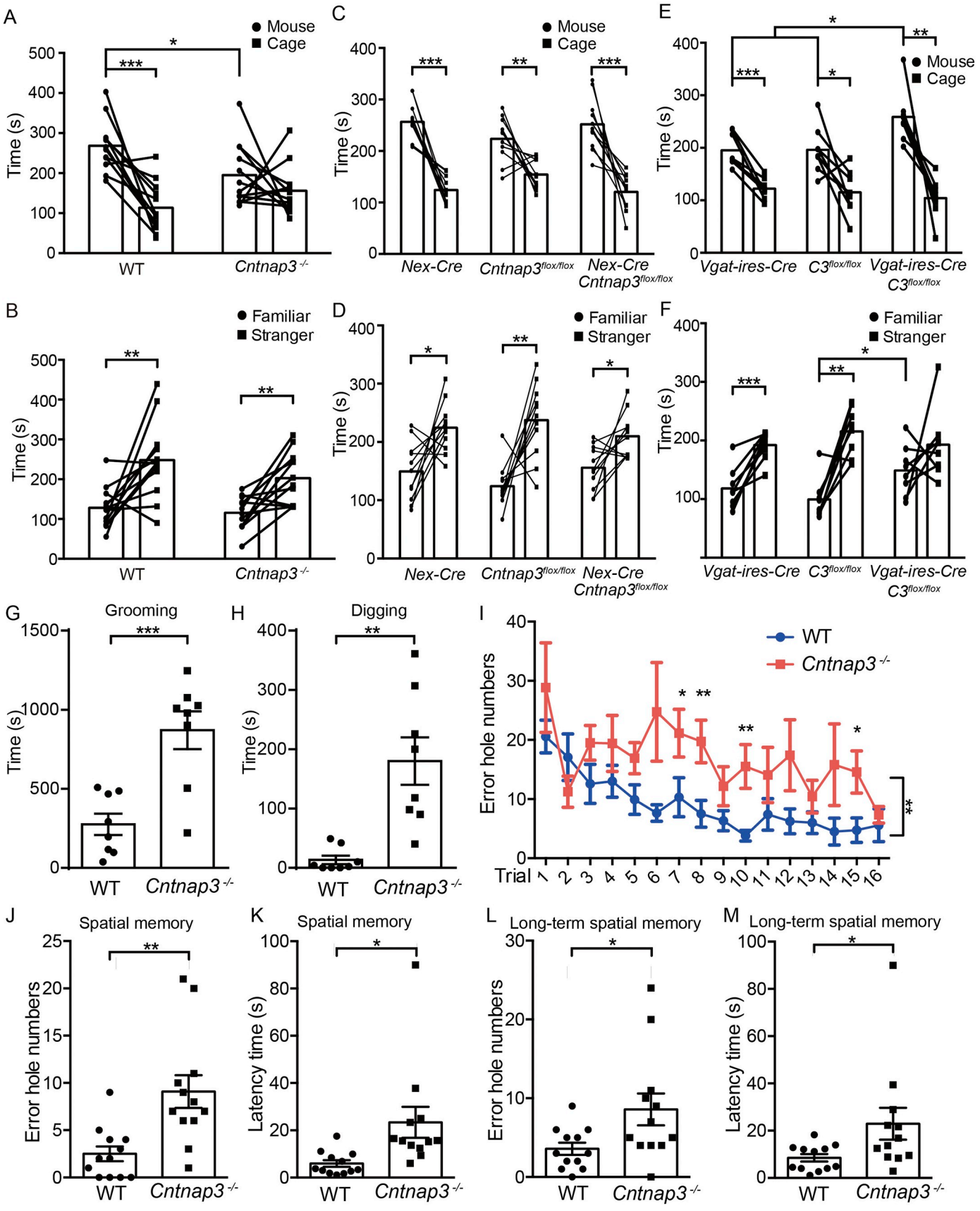

(caption on next page)

Fig. 6. *Cntnap3* KO and conditional KO mice show abnormalities in social behavior, repetitive behaviors and learning memory tasks.
Social behaviors in the three-chamber test (A-F), repetitive test (G, H), learning and memory task in the Barns maze task (I-M). (A) Time interacting with either an unfamiliar mouse or an empty cage within 10 min. (paired t-test, *** $p < .001$, mouse *vs.* cage for each genotype; one-way ANOVA, * $p < .05$, WT *vs.* $Cntnap3^{-/-}$ for mouse or cage). (B) Time interacting with either a stranger mouse or a familiar mouse within 10 min. n = 12 for either $Cntnap3^{-/-}$ or WT mice, (paired t-test, ** $p < 0.01$, familiar *vs.* stranger for each genotype; one-way ANOVA, WT *vs.* $Cntnap3^{-/-}$ for familiar or stranger). (C) Time interacting with either an unfamiliar mouse or an empty cage within 10 min. (paired t-test, *** $p < 0.001$, ** $p < 0.01$, *$p < 0.05$, mouse *vs.* cage for all genotypes; one-way ANOVA, Ctrl *vs. Nex-Cre:* $Cntnap3^{flox/flox}$ for mouse or cage). (D) Time interacting with either a stranger or a familiar mouse in 10 min. $n = 11$ for each genotype, (paired t-test, ** $p < 0.01$, familiar *vs.* stranger for all genotypes; one-way ANOVA, Ctrl *vs. Nex-Cre:* $Cntnap3^{flox/flox}$ for familiar or stranger). (E) Time interacting with either an unfamiliar mouse or an empty cage within 10 min. (paired t-test, *** $p < 0.001$, ** $p < 0.01$, *$p < 0.05$, mouse *vs.* cage for all genotypes; one-way ANOVA, *$p < 0.05$, Ctrl *vs. Vgat-ires-Cre:* $Cntnap3^{flox/flox}$ for mouse or cage) (F) Time interacting with either a stranger mouse or a familiar mouse within 10 min. (n = 8 for each genotype. Paired t-test, ** $p < 0.01$, *** $p < 0.001$, familiar *vs.* stranger for all genotypes; one-way ANOVA, *$p < 0.05$, Ctrl *vs. Vgat-ires-Cre:* $Cntnap3^{flox/flox}$ for familiar or stranger) (G) Time the mice spent to self-grooming in one hour within home cage. ** $p < 0.01$, Student's t-test, WT *vs.* $Cntnap3^{-/-}$. (H) Time the mice spent to digging in one hour within home cage. (n = 8 for either genotype, ** $p < 0.01$, Student's t-test, WT *vs.* $Cntnap3^{-/-}$) (I) Learning curve as indicated by the error hole numbers before entering the hole during a 4-day training period (n = 12 for each genotype. Two-way ANOVA, *$p < 0.05$, ** $p < 0.01$, WT *vs.* $Cntnap3^{-/-}$). The error hole numbers (J) and latency time (up to 90s) (K) before exploring the target hole at the first-test (spatial memory). The error hole numbers (L) and latency time (up to 90s) (M) before exploring the target hole at the second test (long-term spatial memory). *$p < 0.05$, ** $p < 0.01$, Student's t-test, WT *vs.* $Cntnap3^{-/-}$.
Statistical significance was evaluated by Student's t-test, paired *t*-test (three-chamber tests) or two-way ANOVA (curve): *$p < 0.05$, ** $p < 0.01$, *** $p < 0.001$, Error bars: ± SEM.
See also Fig. S6.

including elevated plus maze (Fig. S6 F, G, $n = 8$ mice for either group, Student's t-test), light/dark shuttling (Fig. S6 H, n = 8 mice for either group, Student's t-test), open field test (Fig. S6 I, J, n = 8 mice for either group, Student's t-test), novel object recognition (Fig. S6 K, n = 8 mice for either group, paired t-test), as well as context and cue-dependent fear conditioning (Fig. S6 L, M, N, n = 8 mice for either group, Student's t-test for Fig. S6 L and M, two-way ANOVA for Fig. S6 N). These data suggest that $Cntnap3^{-/-}$ mice have specific defects related to social behaviors, repetitive behaviors, as well as learning and memory, but appeared normal levels of anxiety and fear conditioning responses.

In the excitatory neuron specific knockout mice (*Nex-Cre:* $Cntnap3^{flox/flox}$) and inhibitory neuron specific knockout mice (*Vgat-ires-Cre:* $Cntnap3^{flox/flox}$), we found similar defects in learning curve of the Barnes Maze test (Fig. 7A–D, n = 11 mice (Fig. 7A, B) or n = 8 mice (Fig. 7C, D) for each group, two-way ANOVA, *: $p < 0.05$, **: $p < 0.01$, *Nex-Cre:* $Cntnap3^{flox/flox}$ or *Vgat-ires-Cre:* $Cntnap3^{flox/flox}$ *vs.* $Cntnap3^{flox/flox}$ or Cre), suggesting that proper functions of CNTNAP3 in both excitatory and inhibitory neurons are required for acquiring a certain type of spatial memory. Interestingly, deletion of CNTNAP3 in excitatory neurons exhibited more severe defects in spatial and long-term spatial memory tasks, comparing to inhibitory neurons specific deletion (Fig. 7 *E*-H, Fig. S8 A-D, n = 11 mice (Fig. 7 E-H) or n = 8 mice (Fig. S8 A-D) for each group, owe-way ANOVA, *: $p < 0.05$, **: $p < 0.01$, ***: $p < 0.001$), suggesting that CNTNAP3 may play a more important role in glutamatergic neurons in regulating long-term memory maintenance. Similarly, we did not find any defects in the elevated plus maze or open field test in either excitatory neuron knockout (Fig. S7 C—F, n = 11 mice for each group, owe-way ANOVA), or inhibitory neurons knockout mice (Fig. S7 E-H, n = 8 mice for each group, owe-way ANOVA), suggesting that CNTNAP3 has no effects in regulating anxiety levels.

4. Discussion

We characterized critical functions of the synaptic adhesion molecule CNTNAP3 in synaptic development and transmission, as well as social behavior, repetitive behavior and cognitive tasks. The genetic connections between CNTNAP family and ASD are very intriguing over the years, as other synaptic adhesion molecules are implicated in ASD. R1219X was a stop-gain *de novo* mutation that was found in an ASD patient, which indicated that CNTNAP3 might be an ASD candidate gene. In this study, we proved that R1219X could not interact with PSD-95 or Gephyrin, which were important scaffolding proteins in both excitatory synapses and inhibitory synapses. Moreover, R1219X could not rescue the neuronal morphology and synaptic changes which caused by knocking down *Cntnap3*. These suggest that R1219X may be a *loss-of-function* mutation of CNTNAP3 due to losing the function of its trans member region and intracellular part. Additionally, we identified two transmitted mutations (P614A, R786C) in *CNTNAP3* gene through whole-exome sequencing. Although neither mutation is a *de novo* mutation, we further addressed the functions of each mutations in regarding to synapse development and showed that they were indeed *loss-of-function* variants. But on the other hand, P614A and R786C are point mutations which only cause one amino acid mutation of CNTNAP3. Comparing with the stop-gain mutation of R1219X, the functional changes of P614A and R786C may be more lightly (Fig. 1D). That might be one reason why the fathers who also have the mutation of P614A or R786C are not ASD patients. Our results could only reveal the function of these mutations *in vitro*. As the *in vivo* system is more complicated, the lightly changes must be accumulated or induced by some other factors, for instance, the environmental factors, and then caused the ASD. These data suggested that besides *de novo* mutations, transmitted variants in ASD patients could also significantly contribute to pathophysiology of ASD.

Although *CNTNAP2* and *CNTNAP4* are ASD candidate genes in previous genetic and functional studies, the detail function of CNTNAPs in synapse development is yet to be determined. The finding that CNTNAP3 has interactions with NLGN1/2 family members strongly suggests that CNTNAP3 is an important synaptic adhesion molecule that plays critical roles in regulating synapse development, as confirmed by our experiments (Chih et al., 2005; Varoqueaux et al., 2006). Our data suggest that CNTNAP3 is an essential component of both excitatory synapse and inhibitory synapse. Further work is needed to determine the molecular mechanisms underlying the differentially regulatory function of CNTNAP3 in both excitatory and inhibitory synapses. The finding that CNTNAP3 regulates synapses development differentially provides novel insights for further understanding of the synapse basis for ASD.

Comparing with behavioral defects identified in $Cntnap2^{-/-}$ and $Cntnap4^{-/-}$ mice, we found rather specific defects in social behavior, repetitive behavior and cognitive tasks in $Cntnap3^{-/-}$ mice, suggesting that CNTNAP3 may play a more specific role in regulating social interaction, repetitive behavior, as well as learning and memory in mice. Further work of determining specific neural circuits responsible for defects in social behavior and learning memory would be crucial to provide insights into neural circuits regulating different cognitive behaviors specifically.

> 70% ASD cases include intellectual disability, language deficits, epilepsy, motor abnormalities, anxiety, and gastrointestinal problems. Moreover, a deletion of 9p12 which contains CNTNAP3 was found in one mental retardation (MR) patient (Mosrati et al., 2012). In our experiment, the $Cntnap3^{-/-}$ mice showed the disability of spatial

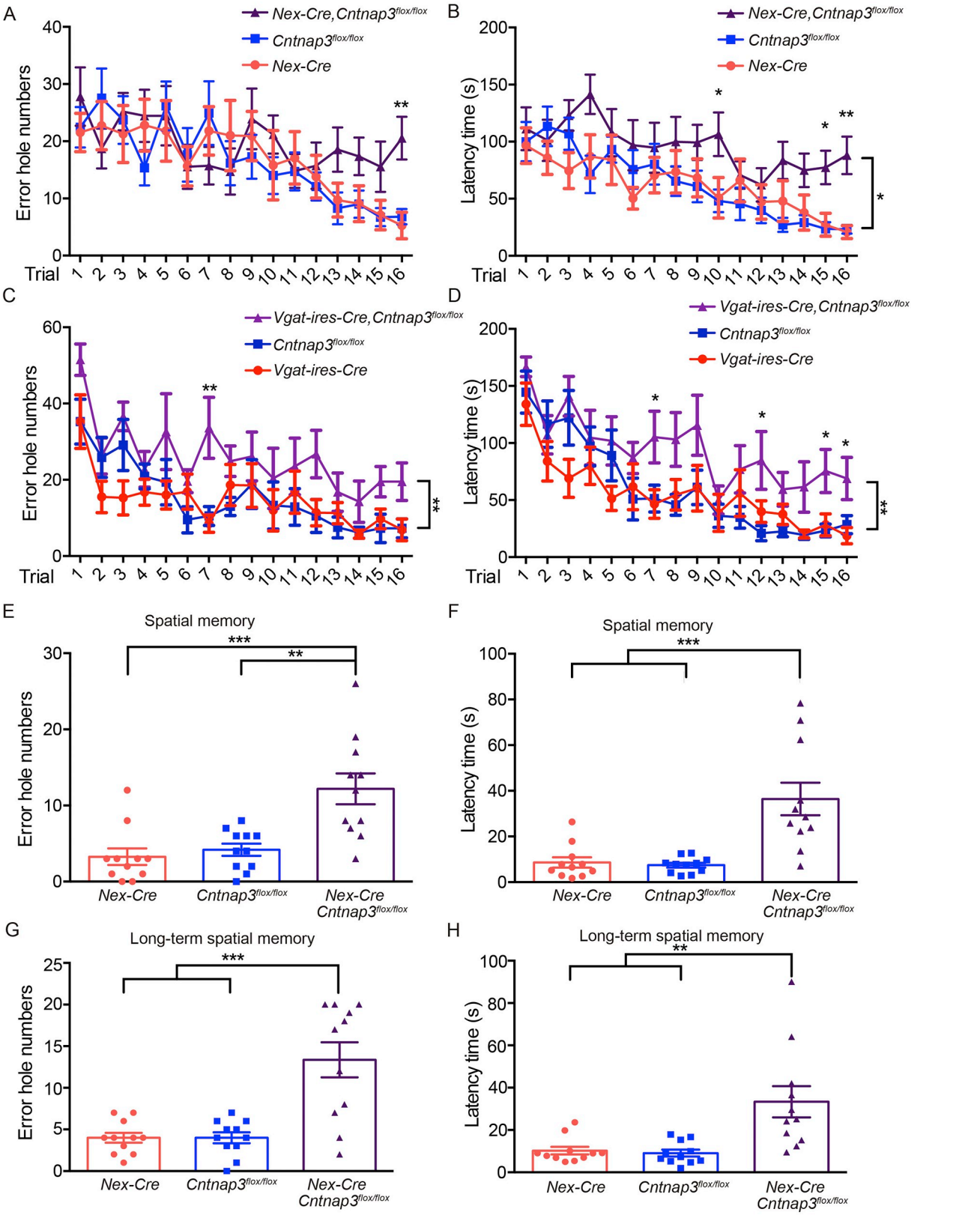

(caption on next page)

Fig. 7. Both excitatory and inhibitory neuron specific deletion of *Cntnap3* exhibited abnormalities in learning and memory tasks.
Learning curve as indicated by the error hole numbers to enter the hole during a 4-day training period (A,C) or indicated by the latency time (up to 180 s) before entering the hole during a 4-day training period (B, D). (A, B) *Nex-Cre*, *Cntnap3*$^{flox/flox}$, (C,D) *vGat-ires-Cre*, *Cntnap3*$^{flox/flox}$. (E-H) Spatial and long-term spatial tasks for *Nex-Cre*, *Cntnap3*$^{flox/flox}$ mice. (E) The error hole number before exploring the target hole at the first-test (spatial memory). (F) The latency time before exploring the target hole (up to 90s) at the first test. (G) The error hole number before exploring the target hole at the second test (long-term spatial memory). (H) The latency time before exploring the target hole (up to 90s) at the second test.
Statistical significance was evaluated by one-way ANOVA, paired t test (three-chamber) or two-way ANOVA (curve): $*p < 0.05$, $** p < 0.01$, $*** p < 0.001$, error bars: ± SEM.
See also Fig. S7 and Fig. S8.

learning and memory. This data suggest us deletion of CNTNAP3 might be one reason of ASD which also has intellectual disability.

Recent evidence implicates synapse changes as important substrates of pathogenesis in ASD. In ASD patients, Golgi-staining showed ASD human brain tissue revealed an increase in spine density by post-mortem (Hutsler and Zhang, 2010). The elevated spine density was also found in the patient with fragile-X syndrome, which was Similar to 'pure' autism (Irwin et al., 2001). In the ASD model mice, the change of synapse density was not exactly the same. The density of excitatory synapses was decreased in the mice deficient in MeCP2; on the other hand, the density of excitatory synapses was increased in the MeCP2 duplicated mice (Chao et al., 2007). The *Cntnap2*$^{-/-}$ mice showed the decreased spine density (Varea et al., 2015). While the spine density of *Fmr1*$^{-/-}$ mice was increased in both apical dendrite and basal dendrite (Dolen et al., 2007). Our data suggest us that then spine density of *Cntnap3*$^{-/-}$ mice were decreased in the S1 and CA1region, which might be one of the reasons induced ASD. Moreover, the density and the function changes of interneurons were also important in ASD. The *Cntnap2*$^{-/-}$ mice showed the decreased inter neuron density, which caused the ASD include epilepsy (Penagarikano et al., 2011). In our experiment, the PV-neuron density of *Cntnap3*$^{-/-}$ was increased in the S1, CA1 and CA3 region and we did not find the phenotype of epilepsy. So these suggest that CNTNAP3 might play a critical role in the ASD include intellectual disability but not epilepsy.

In the Golgi stains, we used the mice of *Nex-Cre:Cntnap3*$^{flox/flox}$ which finished the all of the behavioral tests due to the limitation of littermate mice groups. The behavior of three-chamber test and Barnes Maze might change the spine density of mice during the exploring and training part. In order to avoid the confounder of the data by preceding behavior, we do the Golgi stains 2 weeks after the second Barnes Maze test. It is 3 weeks after the last training of Barnes Maze. It has been reported that in motor learning, the increase in spine elimination ultimately resulted in the total spine density in the trained animals returning to control levels by day 16 (Xu et al., 2009). So we think the spine density has returned to the control level by day 21 after Barnes Maze training. On the other hand, the data of Golgi stains showed that the spine density of adult WT mice (which did not do the behavioral tests) and adult NEX-cre or *Cntnap3*$^{flox/flox}$ mice has no significant change (Fig. 4. A-D, One-way ANOVA). These data suggested that the decreased spine density in *Cntnap3*$^{-/-}$ mice was due to the genotype. However, if CNTNAP3 is involved in the spine formation or elimination induced by social interaction or Barnes Maze training, 3 weeks delay in analysis was not enough to avoid the effect of training. So the decreased spine density in *Nex-Cre:Cntnap3*$^{flox/flox}$ mice might be due to collective effect of genotype and behavioral training.

Combined the genetic mutations we discovered in Chinese Han ASD and Simons simplex collections, as well as functional evidences in genetic engineered mice, we suggest that *CNTNAP3* is an ASD candidate gene and the imbalance of excitatory and inhibitory synapse development caused by mutations of *CNTNAP3* contribute to the abnormal social behavior, repetitive behavior and cognitive functions.

Supplementary data to this article can be found online at https://doi.org/10.1016/j.nbd.2019.104486.

Author contributions

Z.Q designed the study. D.T performed most of the experiment and data analysis. R.C, L.H, X.W performed the electrophysiology experiment. J.L, X.X contributed to *in situ* hybridation experiments. Y.L, W.Z. contributed to the sample collection and NGS analysis for R786C mutation. Y.Z contributed in the mice feeding and genotyping. J S·S contributed in the cell culture. Y.Z. and Y.S.D. contributed the sample collection and NGS analysis for P614A mutations. D.T, R.C and Z.Q wrote the manuscript with the help of all other authors.

Conflict of interests

The authors declare no competing interests.

Acknowledgements

We thank the team of WuXi NextCODE for technical assistance in SSC data analysis. We appreciate obtaining access to genotype, phenotype and pedigree data on SFARI Base. This work was supported by the National Basic Research Program of China (2014CB964600, 2017YFA0105201, 2017YFA0103303, 2017YFA0102601), NSFC Grants (#31625013, #91732302, #81527901, #81471484, #31670842), the Strategic Priority Research Program of the Chinese Academy of Sciences (XDBS01060200, XDA01020309), Shanghai Brain-Intelligence Project from STCSM (16JC1420500), the Open Large Infrastructure Research of Chinese Academy of Sciences, the Program of Shanghai Academic Research Leader (19XD1404300), and the Shanghai Municipal Science and Technology Major Project (2018SHZDZX05).

References

Alarcon, M., Abrahams, B.S., Stone, J.L., Duvall, J.A., Perederiy, J.V., Bomar, J.M., Sebat, J., Wigler, M., Martin, C.L., Ledbetter, D.H., et al., 2008. Linkage, association, and gene-expression analyses identify CNTNAP2 as an autism-susceptibility gene. Am. J. Hum. Genet. 82, 150–159.
Anderson, G.R., Galfin, T., Xu, W., Aoto, J., Malenka, R.C., Sudhof, T.C., 2012. Candidate autism gene screen identifies critical role for cell-adhesion molecule CASPR2 in dendritic arborization and spine development. Proc. Natl. Acad. Sci. U. S. A. 109, 18120–18125.
Arking, D.E., Cutler, D.J., Brune, C.W., Teslovich, T.M., West, K., Ikeda, M., Rea, A., Guy, M., Lin, S., Cook, E.H., et al., 2008. A common genetic variant in the neurexin superfamily member CNTNAP2 increases familial risk of autism. Am. J. Hum. Genet. 82, 160–164.
Ashrafi, S., Betley, J.N., Comer, J.D., Brenner-Morton, S., Bar, V., Shimoda, Y., Watanabe, K., Peles, E., Jessell, T.M., Kaltschmidt, J.A., 2014. Neuronal Ig/Caspr recognition promotes the formation of axoaxonic synapses in mouse spinal cord. Neuron 81, 120–129.
Bakkaloglu, B., O'Roak, B.J., Louvi, A., Gupta, A.R., Abelson, J.F., Morgan, T.M., Chawarska, K., Klin, A., Ercan-Sencicek, A.G., Stillman, A.A., et al., 2008. Molecular cytogenetic analysis and resequencing of contactin associated protein-like 2 in autism spectrum disorders. Am. J. Hum. Genet. 82, 165–173.
Bellen, H.J., Lu, Y., Beckstead, R., Bhat, M.A., 1998. Neurexin IV, caspr and paranodin–novel members of the neurexin family: encounters of axons and glia. Trends Neurosci. 21, 444–449.
Chao, H.T., Zoghbi, H.Y., Rosenmund, C., 2007. MeCP2 controls excitatory synaptic strength by regulating glutamatergic synapse number. Neuron 56, 58–65.
Chih, B., Engelman, H., Scheiffele, P., 2005. Control of excitatory and inhibitory synapse formation by neuroligins. Science 307, 1324–1328.
de la Torre-Ubieta, L., Won, H., Stein, J.L., Geschwind, D.H., 2016. Advancing the understanding of autism disease mechanisms through genetics. Nat. Med. 22, 345–361.

Feng, J., Schroer, R., Yan, J., Song, W., Yang, C., Bockholt, A., Cook, E.J., Skinner, C., Schwartz, C.E., Sommer, S.S., 2006. High frequency of neurexin 1beta signal peptide structural variants in patients with autism. Neurosci. Lett. 409, 10–13.
Hirata, H., Umemori, J., Yoshioka, H., Koide, T., Watanabe, K., Shimoda, Y., 2016a. Cell adhesion molecule contactin-associated protein 3 is expressed in the mouse basal ganglia during early postnatal stages. J. Neurosci. Res. 94, 74–89.
Hirata, H., Takahashi, A., Shimoda, Y., Koide, T., 2016b. Caspr3-deficient mice exhibit low motor learning during the early phase of the accelerated Rotarod task. PLoS ONE 11, e147887.
Huguet, G., Ey, E., Bourgeron, T., 2013. The genetic landscapes of autism spectrum disorders. Annu. Rev. Genomics Hum. Genet. 14, 191–213.
Hutsler, J.J., Zhang, H., 2010. Increased dendritic spine densities on cortical projection neurons in autism spectrum disorders. Brain Res. 1309, 83–94.
Iossifov, I., O'Roak, B.J., Sanders, S.J., Ronemus, M., Krumm, N., Levy, D., Stessman, H.A., Witherspoon, K.T., Vives, L., Patterson, K.E., et al., 2014. The contribution of de novo coding mutations to autism spectrum disorder. Nature 515, 216–221.
Irwin, S.A., Patel, B., Idupulapati, M., Harris, J.B., Crisostomo, R.A., Larsen, B.P., Kooy, F., Willems, P.J., Cras, P., Kozlowski, P.B., et al., 2001. Abnormal dendritic spine characteristics in the temporal and visual cortices of patients with fragile-X syndrome: a quantitative examination. Am. J. Med. Genet. 98, 161–167.
Jamain, S., Quach, H., Betancur, C., Rastam, M., Colineaux, C., Gillberg, I.C., Soderstrom, H., Giros, B., Leboyer, M., Gillberg, C., et al., 2003. Mutations of the X-linked genes encoding neuroligins NLGN3 and NLGN4 are associated with autism. Nat. Genet. 34, 27–29.
Karayannis, T., Au, E., Patel, J.C., Kruglikov, I., Markx, S., Delorme, R., Heron, D., Salomon, D., Glessner, J., Restituito, S., et al., 2014. Cntnap4 differentially contributes to GABAergic and dopaminergic synaptic transmission. Nature 511, 236–240.
Kashani, A.H., Qiu, Z., Jurata, L., Lee, S.K., Pfaff, S., Goebbels, S., Nave, K.A., Ghosh, A., 2006. Calcium activation of the LMO4 transcription complex and its role in the patterning of thalamocortical connections. J. Neurosci. 26, 8398–8408.
Kim, H.G., Kishikawa, S., Higgins, A.W., Seong, I.S., Donovan, D.J., Shen, Y., Lally, E., Weiss, L.A., Najm, J., Kutsche, K., et al., 2008. Disruption of neurexin 1 associated with autism spectrum disorder. Am. J. Hum. Genet. 82, 199–207.
Kong, S.W., Collins, C.D., Shimizu-Motohashi, Y., Holm, I.A., Campbell, M.G., Lee, I.H., Brewster, S.J., Hanson, E., Harris, H.K., Lowe, K.R., et al., 2012. Characteristics and predictive value of blood transcriptome signature in males with autism spectrum disorders. PLoS ONE 7, e49475.
Li, J., Wang, L., Guo, H., Shi, L., Zhang, K., Tang, M., Hu, S., Dong, S., Liu, Y., Wang, T., et al., 2017. Targeted sequencing and functional analysis reveal brain-size-related genes and their networks in autism spectrum disorders. Mol. Psychiatry 22, 1282–1290.
Lim, E.T., Uddin, M., De Rubeis, S., Chan, Y., Kamumbu, A.S., Zhang, X., D'Gama, A.M., Kim, S.N., Hill, R.S., Goldberg, A.P., et al., 2017. Rates, distribution and implications of postzygotic mosaic mutations in autism spectrum disorder. Nat. Neurosci. 20, 1217–1224.
Mosrati, M.A., Schrauwen, I., Kamoun, H., Charfeddine, I., Fransen, E., Ghorbel, A., Van Camp, G., Masmoudi, S., 2012. Genome wide analysis in a family with sensorineural hearing loss, autism and mental retardation. Gene 510, 102–106.
Pagnamenta, A.T., Bacchelli, E., de Jonge, M.V., Mirza, G., Scerri, T.S., Minopoli, F., Chiocchetti, A., Ludwig, K.U., Hoffmann, P., Paracchini, S., et al., 2010. Characterization of a family with rare deletions in CNTNAP5 and DOCK4 suggests novel risk loci for autism and dyslexia. Biol. Psychiatry 68, 320–328.
Peles, E., Nativ, M., Lustig, M., Grumet, M., Schilling, J., Martinez, R., Plowman, G.D., Schlessinger, J., 1997. Identification of a novel contactin-associated transmembrane receptor with multiple domains implicated in protein-protein interactions. EMBO J. 16, 978–988.
Penagarikano, O., Abrahams, B.S., Herman, E.I., Winden, K.D., Gdalyahu, A., Dong, H., Sonnenblick, L.I., Gruver, R., Almajano, J., Bragin, A., et al., 2011. Absence of CNTNAP2 leads to epilepsy, neuronal migration abnormalities, and core autism-related deficits. CELL 147, 235–246.
Poliak, S., Salomon, D., Elhanany, H., Sabanay, H., Kiernan, B., Pevny, L., Stewart, C.L., Xu, X., Chiu, S.Y., Shrager, P., et al., 2003. Juxtaparanodal clustering of shaker-like K + channels in myelinated axons depends on Caspr2 and TAG-1. J. Cell Biol. 162, 1149–1160.
Rios, J.C., Melendez-Vasquez, C.V., Einheber, S., Lustig, M., Grumet, M., Hemperly, J., Peles, E., Salzer, J.L., 2000. Contactin-associated protein (Caspr) and contactin form a complex that is targeted to the paranodal junctions during myelination. J. Neurosci. 20, 8354–8364.
Spiegel, I., Salomon, D., Erne, B., Schaeren-Wiemers, N., Peles, E., 2002. Caspr3 and caspr4, two novel members of the caspr family are expressed in the nervous system and interact with PDZ domains. Mol. Cell. Neurosci. 20, 283–297.
Szatmari, P., Paterson, A.D., Zwaigenbaum, L., Roberts, W., Brian, J., Liu, X.Q., Vincent, J.B., Skaug, J.L., Thompson, A.P., Senman, L., et al., 2007. Mapping autism risk loci using genetic linkage and chromosomal rearrangements. Nat. Genet. 39, 319–328.
Traka, M., Goutebroze, L., Denisenko, N., Bessa, M., Nifli, A., Havaki, S., Iwakura, Y., Fukamauchi, F., Watanabe, K., Soliven, B., et al., 2003. Association of TAG-1 with Caspr2 is essential for the molecular organization of juxtaparanodal regions of myelinated fibers. J. Cell Biol. 162, 1161–1172.
Traut, W., Weichenhan, D., Himmelbauer, H., Winking, H., 2006. New members of the neurexin superfamily: multiple rodent homologues of the human CASPR5 gene. Mamm. Genome 17, 723–731.
Turner, T.N., Coe, B.P., Dickel, D.E., Hoekzema, K., Nelson, B.J., Zody, M.C., Kronenberg, Z.N., Hormozdiari, F., Raja, A., Pennacchio, L.A., et al., 2017. Genomic patterns of De novo mutation in simplex autism. Cell 171, 710–722.
Vaags, A.K., Lionel, A.C., Sato, D., Goodenberger, M., Stein, Q.P., Curran, S., Ogilvie, C., Ahn, J.W., Drmic, I., Senman, L., et al., 2012. Rare deletions at the neurexin 3 locus in autism spectrum disorder. Am. J. Hum. Genet. 90, 133–141.
Varea, O., Martin-de-Saavedra, M.D., Kopeikina, K.J., Schürmann, B., Fleming, H.J., Fawcett-Patel, J.M., Bach, A., Jang, S., Peles, E., Kim, E., Penzes, P., 2015. Synaptic abnormalities and cytoplasmic glutamate receptor aggregates in contactin associated protein-like 2/Caspr2 knockout neurons. Proc. Natl. Acad. Sci. U. S. A. 112 (19), 6176–6181.
Varoqueaux, F., Aramuni, G., Rawson, R.L., Mohrmann, R., Missler, M., Gottmann, K., Zhang, W., Sudhof, T.C., Brose, N., 2006. Neuroligins determine synapse maturation and function. Neuron 51, 741–754.
Wen, Z., Cheng, T.L., Li, G.Z., Sun, S.B., Yu, S.Y., Zhang, Y., Du, Y.S., Qiu, Z., 2017. Identification of autism-related MECP2 mutations by whole-exome sequencing and functional validation. Mol. Autism. 8, 43.
Willsey, A.J., State, M.W., 2015. Autism spectrum disorders: from genes to neurobiology. Curr. Opin. Neurobiol. 30, 92–99.
Xu, T., Yu, X., Perlik, A.J., Tobin, W.F., Zweig, J.A., Tennant, K., Jones, T., Zuo, Y., 2009. Rapid formation and selective stabilization of synapses for enduring motor memories. Nature 462, 915–919.
Yu, X., Malenka, R.C., 2003. Beta-catenin is critical for dendritic morphogenesis. Nat. Neurosci. 6, 1169–1177.